Computational and Structural Biotechnology Journal 19 (2021) 37–50

COMPUTATIONAL AND STRUCTURAL BIOTECHNOLOGY JOURNAL

journal homepage: www.elsevier.com/locate/csbj

In silico and *in vitro* insights into tyrosinase inhibitors with a 2-thioxooxazoline-4-one template

Inkyu Choi [a,1], Yujin Park [a,1], Il Young Ryu [a,1], Hee Jin Jung [a], Sultan Ullah [b], Heejeong Choi [a], Chaeun Park [a], Dongwan Kang [a], Sanggwon Lee [a], Pusoon Chun [c], Hae Young Chung [a], Hyung Ryong Moon [a,*]

[a] College of Pharmacy, Pusan National University, Busan 46241, South Korea
[b] Department of Molecular Medicine, The Scripps Research Institute, FL 33458, USA
[c] College of Pharmacy and Inje Institute of Pharmaceutical Sciences and Research, Inje University, Gimhae, Gyeongnam 50834, South Korea

ARTICLE INFO

Article history:
Received 6 October 2020
Received in revised form 1 December 2020
Accepted 2 December 2020
Available online 11 December 2020

Keywords:
Tyrosinase
2-thioxooxazoline-4-one
Anti-melanogenesis
Kojic acid
Docking simulation
β-phenyl-α,β-unsaturated carbonyl scaffold

ABSTRACT

The β-phenyl-α,β-unsaturated carbonyl (PUSC) scaffold confers tyrosinase inhibitory activity, and in the present study, 16 (*Z*)-5-(substituted benzylidene)-3-phenyl-2-thioxooxazolidin-4-one analogues containing this scaffold were synthesized. Mushroom tyrosinase inhibitory activities were examined. Compound **1c** (IC_{50} = 4.70 ± 0.40 μM) and compound **1j** (IC_{50} = 11.18 ± 0.54 μM) inhibited tyrosinase by 4.9 and 2.1-fold, respectively, and did so more potently than kojic acid (IC_{50} = 23.18 ± 0.11 μM). Kinetic analysis of tyrosinase inhibition revealed that **1c** and **1j** inhibited tyrosinase competitively. Results of docking simulation with mushroom tyrosinase using four docking programs suggested that **1c** and **1j** bind more strongly than kojic acid to the active site of tyrosinase and supported kinetic findings that both compounds are competitive inhibitors. The docking results of human tyrosinase homology model indicated that **1c** and **1j** can also strongly inhibit human tyrosinase. EZ-cytox assays revealed **1c** and **1j** were not cytotoxic to B16F10 melanoma cells. The effects of **1c** and **1j** on cellular tyrosinase activity and melanin production were also investigated in α-MSH- and IBMX-co-stimulated these cells. Both compounds significantly and dose-dependently reduced tyrosinase activity, and at 10 μM were more potent than kojic acid at 20 μM. Compounds **1c** and **1j** also inhibited melanogenesis, which suggested that the inhibitory effects of these compounds on melanin production were mainly attributable to their inhibitions of tyrosinase. These results indicate that compounds **1c** and **1j** with the PUSC scaffold have potential use as whitening agents for the treatment of hyperpigmentation-associated diseases.

1. Introduction

Melanin largely determines the color of bird feathers and the skins of mammals and affects the browning of apples, potatoes, and mushrooms [1-5]. In humans, melanin colors hair, eyes, and skin. Melanin protects skin by blocking UV radiation, which produces reactive oxygen species (ROS) [6-9], causes DNA damage, and can cause skin cancer [10-15].

Skin color is considered important in the contexts of fashion and beauty, but the overproduction of melanin due to, for example, excessive UV exposure results in hyperpigmentation, spots, freckles, and melasma [16-20]. Melanin is biosynthesized in the melanosomes of melanocytes by complicated enzymatically driven processes. Three enzymes are primarily involved, namely, tyrosinase and two tyrosinase-related proteins, TYRP1 and TYRP2 [7]. Tyrosinase is the key rate-limiting enzyme of the conversion of L-tyrosine to dopaquinone via L-dopa, and thus, influences melanin biosynthesis in melanocytes [6,21]. Depending on the presence of thiols, such as glutathione and L-cysteine, dopaquinone can act in two different ways [22]. First, it can react with thiols by a Michael addition and be converted to pheomelanin, which is yellow–red colored [22]. Alternatively, in the absence of thiols, dopaquinone is transformed to eumelanin, which is brown-black colored [23,24]. Thus, human skin color is largely determined by the proportions and amounts of eumelanin and pheomelanin in skin [25,26].

Numerous attempts have been made to reduce the production of melanin. These approaches include tyrosinase inhibition, the suppression of melanin transfer from melanocytes to

* Corresponding author at: Laboratory of Medicinal Chemistry, College of Pharmacy, Pusan National University, Busan 46241, Republic of Korea.
E-mail address: mhr108@pusan.ac.kr (H.R. Moon).
[1] These authors (I. Choi, Y. Park, and I.Y. Ryu) contributed equally to this work.

https://doi.org/10.1016/j.csbj.2020.12.001

keratinocytes, and interventions that target intracellular signals for melanogenesis [27]. Although many different natural and synthetic substances have exhibited meaningful anti-melanogenic effects in cell-based assays [28-34], the majority have side effects, such as an insufficient potency, carcinogenic effects, permanent depigmentation, and dermatitis, *in vivo*, in animal models and in humans [35]. Although hydroquinone and kojic acid are used as whitening agents at limited concentrations in a few countries, these skin-lightening agents are prohibited in most countries due to the risks of undesirable side effects, such as possible carcinogenic effects in thyroid [7], nephrotoxicity [6], genotoxicity [36], and cytotoxic effects on melanocytes [6]. Arbutin is α-D-glucopyranoside of hydroquinone that occurs naturally in the bearberry plant of the genus *Arctostaphylos*. Due to its lesser side effects, arbutin is more widely used as a whitening agent than hydroquinone, and its anti-melanogenic effect is known to be due to tyrosinase inhibition. Arbutin is hydrolyzed to hydroquinone and D-glucose by skin microflora, such as *Staphylococcus epidermidis* and *Staphylococcus aureus* [22], by enzymes like α-glycosidase, and by temperature (10% decomposition after 5 days at 20 °C) [37]. Therefore, there is a need for novel tyrosinase inhibitors that are non-carcinogenic and more clinically effective.

Many researchers are trying to discover new tyrosinase inhibitors by exploring new scaffolds and repositioning of old scaffolds including thiourea [38]. Compounds with the 2-thioxooxazolidin-4-one template exhibit many biological activities such as anti-cancer [39], HIV-1 fusion inhibiting [40], 17β-hydroxysteroid dehydrogenase type 3 inhibiting [41], and glucose and triglyceride-lowering activities [42], but have not been reported to exhibit tyrosinase inhibitory activity. Over the past ten years, we reported a variety of compounds with β-phenyl-α,β-unsaturated carbonyl (PUSC) scaffold that have demonstrated excellent inhibition of tyrosinase *in vitro* and *in vivo* [32,34,43-47]. Therefore, we were interested in an incorporating a 2-thioxooxazolidin-4-one template with different benzaldehydes to produce a PUSC scaffold (Fig. 1). According to our accumulated structure–activity relationship data [45,46,48-54], derivatives with a hydroxyl group on the β-phenyl ring of the PUSC scaffold generally have high tyrosinase inhibitory activities. Furthermore, the numbers and positions of hydroxyl groups appear to be closely responsible for the tyrosinase inhibitory efficacy. Accordingly, in the present study, we designed derivatives with various substituents at different positions on the β-phenyl ring of the PUSC scaffold, and subsequently synthesized a series of (*Z*)-5-(substituted benzylidene)-3-phenyl-2-thioxooxazolidin-4-one derivatives. We then evaluated the abilities of derivatives to inhibit mushroom tyrosinase and to suppress tyrosinase activity and melanin production in B16F10 melanoma cells, and also performed kinetic studies and docking simulations to determine how these derivatives interact with tyrosinase.

2. Results and discussion

2.1. Chemistry

The strategy used to synthesize the desired derivatives, (*Z*)-5-(substituted benzylidene)-3-phenyl-2-thioxooxazolidin-4-ones, involved the use of 3-phenyl-2-thioxooxazolidin-4-one as a key template for the construction of the PUSC scaffold (Fig. 1). As depicted in Scheme 1, reaction of ethyl glycolate with phenyl isothiocyanate gave the key intermediate, 3-phenyl-2-thioxooxazolidin-4-one (**2**), in a 29% yield. Sixteen benzaldehydes were refluxed with this intermediate in the presence of acetic acid and sodium acetate to give the final compounds **1a**–**1p** in yields of 18–85%. None of these compounds, with the exception of **1i**, which is a 17β-hydroxysteroid dehydrogenase type 3 inhibitor, has been previously described [41]. Thermodynamically more stable *Z*-isomers were predominately generated. As described by Nair and co-workers [55], the *E*-/*Z*-configuration was determined using vicinal ^{1}H, ^{13}C-coupling constants in proton-coupled ^{13}C spectra. As shown in Fig. 2, vicinal coupling constants between the amide carbonyl C-atom C(1) and the olefinic H-atom at C(3) depend on the geometry of the double bond ((*E*)-isomer: $^{3}J_{cis}$ = 6.8 Hz, (*Z*)-isomer: $^{3}J_{trans}$ = 11.5 Hz). Different vicinal ^{1}H, ^{13}C-coupling constants of geometric isomers are observed in many compounds, including 5-membered and 6-membered exocyclic compounds. The values of $^{3}J_{cis}$ range from 3.6 to 6.4 Hz, whereas the range of values of $^{3}J_{trans}$ values is roughly twice as large (generally > 10 Hz). ^{13}C NMR of compound **1b** was measured in proton-coupled ^{13}C mode, and the ^{3}J value of C4 in **1b** was 3.5 Hz (Refer to Fig. S52 in Supplementary data), suggesting a (*Z*)-configuration.

Chemical shifts of vinylic protons were analyzed based on consideration of the NMR solvent used and the positions and types of substituents on the β-phenyl ring. The chemical shifts of vinylic protons appeared at 6.76 ~ 7.10 ppm. The chemical shifts (6.76 ~ 6.81 ppm) of vinylic protons without a substituent at the 2-position of the β-phenyl ring generally appeared up-field in $CDCl_3$ compared to those (6.82 ~ 6.95 ppm) in DMSO d_6. The presence of highly electronegative elements, such as hydroxyl, methoxyl, and fluoro group at the 2-position of the β-phenyl ring moved the chemical shift of the vinylic proton down-field (**1c**, **1 h**, **1j** and **1p** *vs.* the remaining compounds). In the case of compound **1p**, which had a highly electronegative fluoro substituent at the 2-position of the β-phenyl ring, the chemical shift of the vinylic proton in $CDCl_3$ solvent appeared at 7.08 ppm, which was 0.27 ~ 0.32 ppm higher than the chemical shifts of vinylic protons in other compounds measured in the same solvent. On the other hand, the two hydroxyl groups of **1c** moved 6′-H down-field (7.82 ppm), and the two fluoro substituents of **1p** moved 6′-H more strongly down-field (8.28 ppm). The ^{1}H NMR spectrum of **1p** showed characteristic coupling patterns of the two fluoro substituents. 6′-H appeared as a triplet of doublets due to coupling by the two fluorine atoms and 5′-H. 3′-H and 5′-H also appeared as a triplet of doublets by coupling to the fluorine atoms and vicinal hydrogen atoms. The results of characteristic coupling by fluorine atoms were observed in ^{13}C NMR spectrum of **1p**. All carbon peaks of β-phenyl rings attached to fluorine atoms appeared as doublet of doublets and the ββ-carbon of the PUSC scaffold was also split into a doublet by the 2-fluorine atom.

2.2. Inhibitory activities of thioxazolidinedione derivatives *1a*–*1p* against mushroom tyrosinase

To select derivatives for cell-based assays of anti-melanogenic and tyrosinase-inhibitory effects, the inhibitory activities of the sixteen synthesized (*Z*)-5-(substituted benzylidene)-3-phenyl-2-thioxooxazolidin-4-one analogues, **1a**–**1p**, were examined using mushroom tyrosinase and kojic acid (the positive control with known potent tyrosinase inhibitory activity). All compounds and kojic acid were tested at a concentration of 25 μM. Tyrosinase inhibitory results are shown in Table 1.

Of the sixteen synthesized compounds, two derivatives **1c** (78.05 ± 4.03% inhibition) with a 2,4-dihydroxyl substituent and **1j** (71.12 ± 0.71% inhibition) with a 2-hydroxyl substituent exhibited more potent tyrosinase-inhibition than kojic acid (58.09 ± 5.82% inhibition), and compound **1b** exhibited a moderate inhibitory effect (30.57 ± 1.77% inhibition). Although compound **1a** (10.25 ± 2.36% inhibition) with a 4-hydroxyphenyl only weakly inhibited tyrosinase, the introduction of an additional 3-hydroxyl group into the β-phenyl ring enhanced tyrosinase inhibitory activity to 30.57%

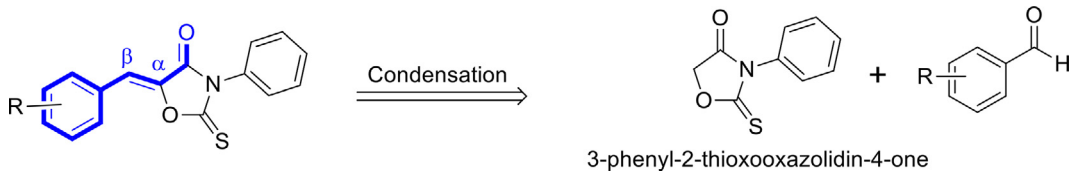

Fig. 1. Synthetic strategy of (*Z*)-5-(substituted benzylidene)-3-phenyl-2-thioxooxazolidin-4-one derivatives possessing the (*E*)-β-phenyl-α,β-unsaturated carbonyl scaffold.

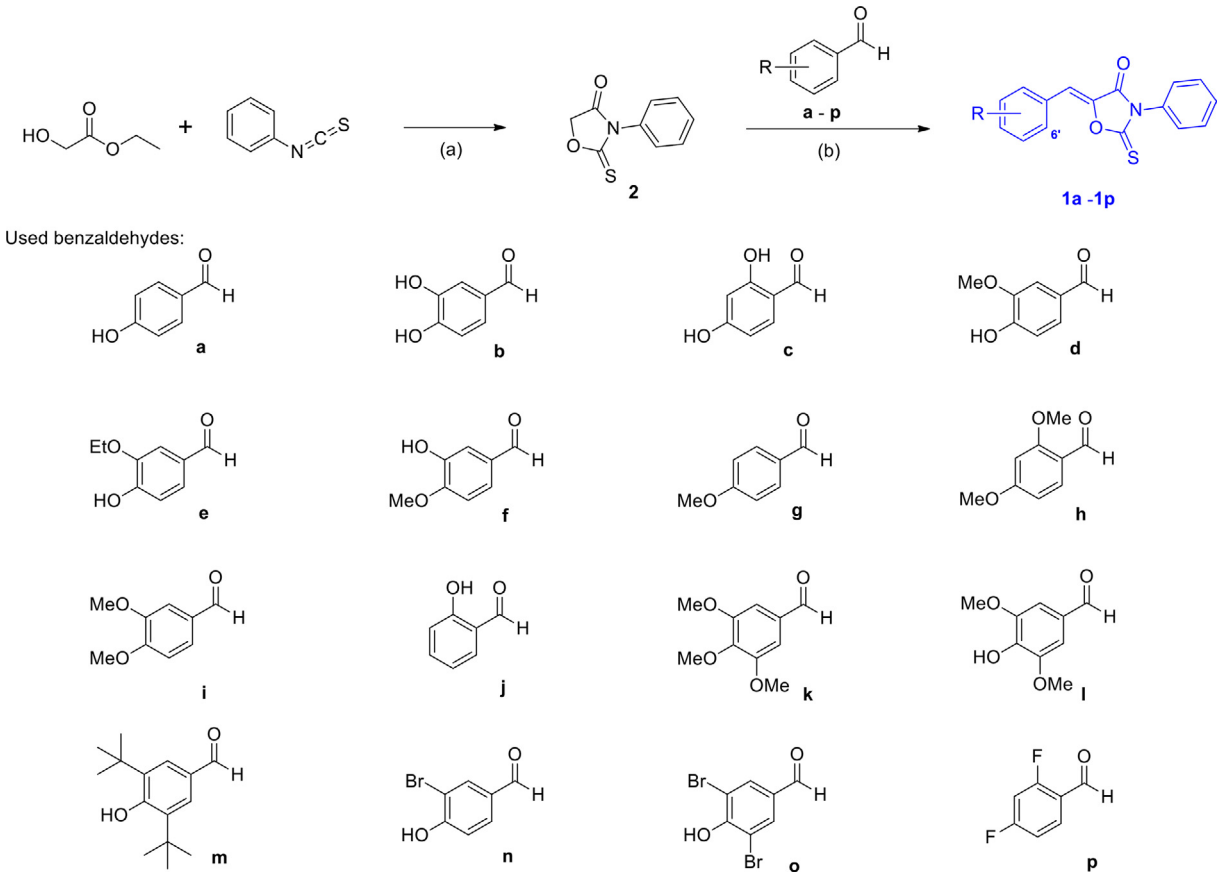

Scheme 1. Synthesis of (*Z*)-5-(substituted benzylidene)-3-phenyl-2-thioxooxazolidin-4-one derivatives **1a**–**1p**. Reagents and conditions: (a) Et_3N, CH_2Cl_2, rt, 42 h, 29.3%; (b) NaOAc, AcOH, reflux, 9–25 h, 18–85%.

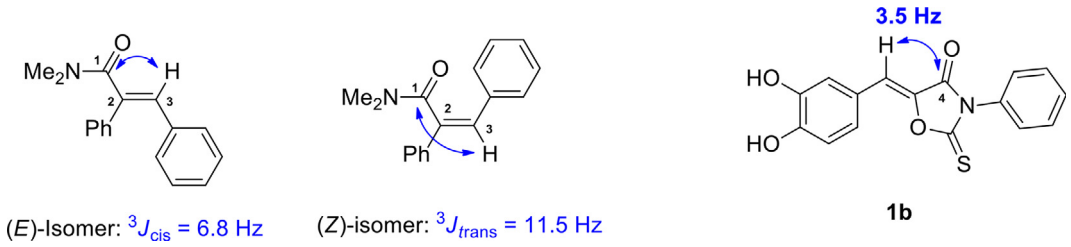

Fig. 2. Relationship between the C,H-spin-coupling constants over three bonds indicated by the arrow and the geometry of the double bond.

(see compound **1b**). Furthermore, the insertion of an additional 2-hydroxyl group into the β-phenyl ring of **1a** increased the tyrosinase inhibitory activity to 78% (**1a** *vs.* **1c**). On the contrary, the introduction of methoxyl or ethoxyl at the 3-position of the β-phenyl ring eliminated tyrosinase inhibitory activity (**1a** *vs.* **1d** and **1e**). Derivatives (**1 h**, **1i**, and **1 k**) without a hydroxyl group on the β-phenyl ring exhibited very weak or no inhibition. The insertion of a 3-bromo group into the β-phenyl ring of **1a** increased tyrosinase inhibitory activity (**1a** *vs.* **1n**) to 25%, while the introduction of substituents (3,5-dimethoxy, 3,5-di-*tert*-butyl, and 3,5-dibromo substituents) at both 3- and 5-positions in the β-phenyl ring did not enhance inhibitory activities (**1a** *vs.* **1 l**, **1 m**, and **1o**). These results indicate hydroxyl groups on the β-phenyl ring are necessary for tyrosinase inhibition and that the number and position of substituents, especially hydroxyl groups, markedly influence tyrosinase inhibitory activity.

Derivative **1c** with a 2,4-dihydroxyphenyl group was the most potent inhibitor of tyrosinase. To investigate whether the hydrogen

Table 1
Mushroom tyrosinase inhibition of the synthesized (*Z*)-5-(substituted benzylidene)-3-phenyl-2-thioxooxazolidin-4-one derivatives **1a**–**1p** and kojic acid.

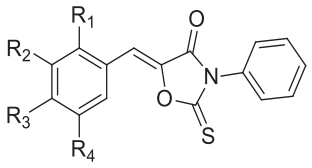

1a -1p

Compound	R_1	R_2	R_3	R_4	Tyrosinase inhibition (%)[a]
1a	H	H	OH	H	10.25 ± 2.36
1b	H	OH	OH	H	30.57 ± 1.77
1c	OH	H	OH	H	78.05 ± 4.03
1d	H	OMe	OH	H	NI[b]
1e	H	OEt	OH	H	NI
1f	H	OH	OMe	H	13.39 ± 9.67
1g	H	H	OMe	H	NI
1h	OMe	H	OMe	H	4.09 ± 3.66
1i	H	OMe	OMe	H	7.47 ± 5.52
1j	OH	H	H	H	71.12 ± 0.71
1k	H	OMe	OMe	OMe	NI
1l	H	OMe	OH	OMe	10.22 ± 4.82
1m	H	*t*-Bu	OH	*t*-Bu	8.53 ± 2.25
1n	H	Br	OH	H	24.96 ± 4.72
1o	H	Br	OH	Br	NI
1p	F	H	F	H	NI
Kojic acid					58.09 ± 5.82

[a]Tyrosinase inhibitions of the synthesized compounds and kojic acid were evaluated at 25 μM using L-tyrosine as a substrate. [b]NI: no inhibition. Results are expressed as means ± SEMs.

bond donor or acceptor characteristics of the hydroxyl groups are associated with tyrosinase inhibition, compound **1p** with a 2,4-difluorophenyl group was synthesized as a congener of **1c**, which possessed a 2,4-dihydroxyphenyl. Unlike a hydroxyl group, fluorine can only serve as a hydrogen bond acceptor. Tests showed **1p** had no mushroom tyrosinase inhibitory activity. Compound **1 h**, which had 2,4-dimethoxyl groups that only act as hydrogen bond acceptors, exhibited very weak tyrosinase inhibition. These results suggest substituents that can act as hydrogen bond acceptors and donors at the 2- and 4-positions of the β-phenyl group, or that can serve as hydrogen bond donors, may play a more important role in tyrosinase enzyme inhibition than substituents capable of acting as hydrogen bond acceptors only at same positions. This suggestion is supported by the pharmacophore results obtained using LigandScout based on AutoDock 4, which showed hydroxyl substituents at the 2- and 4-positions of the β-phenyl group form a hydrogen bond with amino acid residues of Asn260 or Met280 at the active site of tyrosinase, respectively, and that the hydroxyls serve as hydrogen bond donors (Fig. 5). Taken together, the hydroxyl substituents at the 2- and 4-positions of the β-phenyl group play a key role in tyrosinase enzyme inhibition, and the effect on the tyrosinase inhibitory activity is due to the ability of the hydrogen bond donor of hydroxyls.

We also investigated the IC_{50} values of compounds **1c** and **1j**, which more potently inhibited mushroom tyrosinase than kojic acid, and compound **1b**, which moderately inhibited tyrosinase. All four compounds dose-dependently inhibited mushroom tyrosinase (data not shown). The low IC_{50} values of **1c** (4.70 ± 0.40 μM) and **1j** (11.18 ± 0.54 μM) indicated that these compounds inhibited tyrosinase activity more strongly than kojic acid (IC_{50} = 23.18 ± 0. 11 μM), more specifically, the inhibitory potencies of **1c** and **1j** were 5- and 2-fold greater, respectively, than that of kojic acid. On the other hand, the IC_{50} value of compound **1b**, which possessed a catechol group, was 53.38 ± 0.39 μM, indicating poorer mushroom tyrosinase inhibitory activity than kojic acid.

*2.3. Studies on the action of mode of compounds **1c**, and **1j***

To examine the inhibitory modes of action of compounds **1c** and **1j**, we performed a kinetic study on mushroom tyrosinase in the presence of **1c** or **1j** using L-tyrosine as a substrate. Mechanisms of tyrosinase inhibition were investigated by Lineweaver-Burk plot analysis as depicted in Fig. 3. Lineweaver-Burk plots of **1c** or **1j** were similar (Fig. 3a *vs.* b). For each compound, lines produced at different concentrations converged at one point on the y-axis. As the concentrations of **1c** and **1j** were increased, K_M values for tyrosinase dose-dependently increased without changing V_{max} values. These results imply that **1c** and **1j** competitively inhibited tyrosinase and that they bind to the same binding pocket as the tyrosinase substrate, L-tyrosine. The kinetics of these inhibitions (Table 2) showed the following: for **1c**; $K_i = 3.02 \times 10^{-6}$, 2.51×10^{-6}, and 2.19×10^{-6} M at 2.5, 5.0, and 10.0 μM, respectively; and for **1j**; $K_i = 5.85 \times 10^{-6}$, 4.51×10^{-6}, and 3.22×10^{-6} M at 5.0, 10.0, and 20.0 μM, respectively. K_M values of **1c** at concentrations of 2.5, 5.0, and 10.0 μM were 6.56, 10.72, and 19.93 mM, respectively, and those of **1j** at concentrations of 5.0, 10.0 and 20.0 μM were 5.47, 9.48, and 21.26 mM, respectively. Compounds **1c**, and **1j** had similar V_{max} values of 4.0×10^{-2} and 2.7×10^{-2} mM/min, respectively, regardless of concentration.

*2.4. Docking simulation studies of compounds **1c** and **1j** and kojic acid with mushroom tyrosinase*

To investigate whether the synthesized (*Z*)-5-(substituted benzylidene)-3-phenyl-2-thioxooxazolidin-4-ones can bind directly to the active site of tyrosinase, docking simulations were performed using AutoDock Vina 1.1.2 software (developed by The Scripps Research Institute). Two compounds, **1c**, and **1j**, with highest inhibitory activity against mushroom tyrosinase were selected as ligands for the docking simulation. After energy minimization of 2D-structures using Chem3D Pro 12.0 software (Cam-

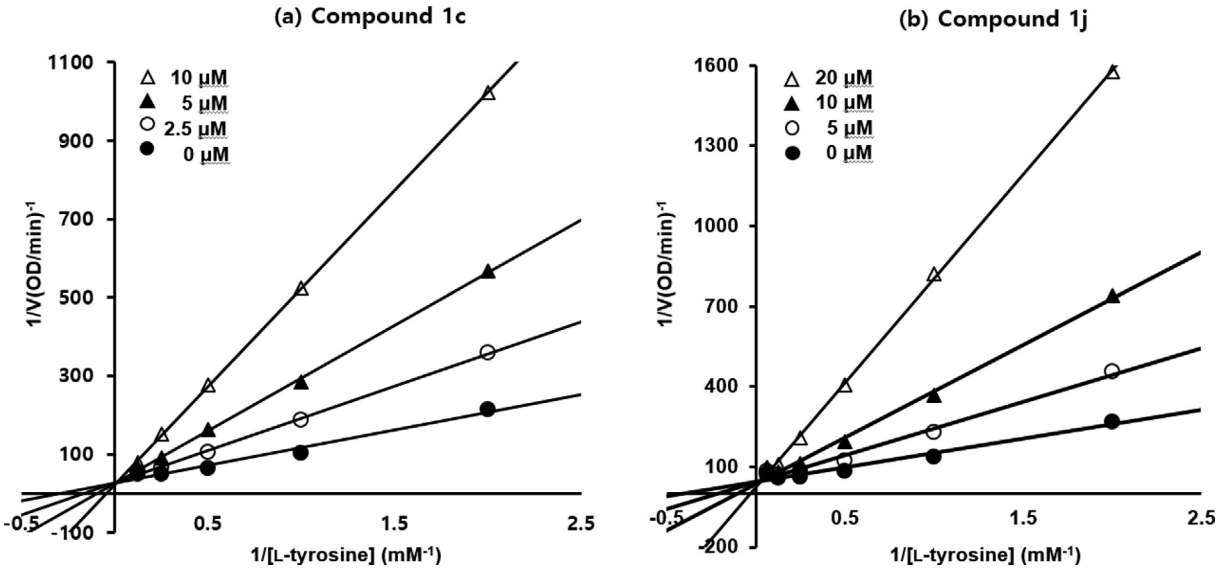

Fig. 3. Lineweaver-Burk plots for the inhibition of mushroom tyrosinase activity by (*Z*)-5-(substituted benzylidene)-3-phenyl-2-thioxooxazolidin-4-one derivatives (a) **1c** and (b) **1j**. Inhibition types were investigated using Lineweaver-Burk plots. Data are shown as mean values of 1/V, defined as the inverse of increased absorbance at 475 nm per min as determined by three independent experiments at five different L-tyrosine concentrations. Concentrations of **1c** were 0 μM (filled circles), 2.5 μM (unfilled circles), 5.0 μM (filled triangles), and 10.0 μM (unfilled triangles) and the concentrations of **1j** were 0 μM (filled circles), 5.0 μM (unfilled circles), 10.0 μM (filled triangles), and 20.0 μM (unfilled triangles). The modified Michaelis-Menten equation was used: $1/V_{max} = (1/K_M)(1 + [S]/K_i)$, where V_{max} is maximum reaction rate, K_M is a Michaelis-Menten constant, [S] is L-tyrosine concentration, and K_i is the inhibition constant. All experiments were independently performed in triplicate.

Table 2
Kinetic analysis of compounds **1c**, and **1j**.

Inhibitor							
1c				**1j**			
Conc.	V_{max} (mM/min)	K_M (mM)	K_i (M)	Conc.	V_{max} (mM/min)	K_M (mM)	K_i (M)
2.5 μM	4.0×10^{-2}	6.56	3.02×10^{-6}	5.0 μM	2.7×10^{-2}	5.47	5.85×10^{-6}
5.0 μM	4.0×10^{-2}	10.72	2.51×10^{-6}	10.0 μM	2.7×10^{-2}	9.48	4.51×10^{-6}
10.0 μM	4.0×10^{-2}	19.93	2.19×10^{-6}	20.0 μM	2.7×10^{-2}	21.26	3.22×10^{-6}

Data are mean values of 1/V (inverse of the increase in absorbance at a wavelength of 475 nm per min (ΔA_{475}/min)), of three independent experiments conducted using different L-tyrosine concentrations. The Lineweaver-Burk plot equation is: $1/V = 1/V_{max} + K_M/V_{max} \times 1/[S]$ and the modified Michaelis-Menten equation is $1/V_{max} = (1 + [I]/K_i) \times 1/K_M$, where V is the reaction rate, V_{max} is the maximum reaction rate, K_M is the Michaelis-Menten constant, [S] is substrate concentration, [I] is inhibitor concentration, and K_i is the inhibition constant.

bridgeSoft Corporation), 3D-structures of the two compounds were created. Tyrosinase of *Agaricus bisporus* (a species of mushroom) was utilized as the 3D-structure [Protein Data Bank (PDB) ID: 2Y9X] for docking simulation. Although the correlation between the binding affinities of the two ligands and their abilities to inhibit mushroom tyrosinase was not perfect, both derivatives had much stronger binding affinities (−7.3 ~ −7.5 kcal/mol) than the kojic acid (−5.7 kcal/mol) (Fig. 4d). LigandScout 4.3 software was utilized to determined which amino acid residues of tyrosinase interacted with **1c** and **1j**. Three amino acids (His259, His263, and Met280) of tyrosinase were found to interact with kojic acid (Fig. 4c). The branched hydroxyl group of kojic acid formed two hydrogen bonds with amino acid residues His259 and His263 and the ring hydroxyl formed a hydrogen bond with Met280. Both hydroxyl groups of kojic acid acted as hydrogen bonding donors. Compounds **1c** and **1j** both interacted hydrophobically with five amino acid residues (Val248, Met257, Phe264, Val283, and Ala286) (Fig. 4a and b) without hydrogen bonding. Docking simulation results suggested although the amino acids that interacted with kojic acid and those that interacted with **1c** and **1j** differed all three ligands bind to the active site of tyrosinase. However, LigandScout results based on AutoDock Vina docking simulations showed kojic acid appeared to bind more strongly to the active site of tyrosinase than **1c** or **1j**, which was contrary to the results of the binding affinity obtained from AutoDock Vina.

Two more docking simulation software packages, that is, AutoDock 4 and Dock 6, were utilized to increase the reliability of docking simulation results. The same tyrosinase species used for the AutoDock Vina simulation were used. According to AutoDock 4 and Dock 6, the binding affinities of **1c** were −7.41 and −30.70 kcal/mol and for **1j** were −7.19 and −32.42 kcal/mol, respectively (Fig. 5b), which were greater than those of kojic acid (−4.2 and −27.59 kcal/mol, respectively). Furthermore, these results were consistent with experimental data for mushroom tyrosinase inhibition. However, according to Dock 6, **1j** had greater binding affinity than **1c**, while in AutoDock 4, the reverse was the case. Compound **1c** which showed greater inhibitory activity against mushroom tyrosinase than **1j** showed higher binding affinity to tyrosinase than **1j** in AutoDock 4. Thus, LigandScout results based on AutoDock 4 were examined (Fig. 5a). These results showed kojic acid formed one hydrogen bond with Met280 and that its ring interacted with His263 by π-π stacking. Compound **1c** which showed stronger binding affinity than compound **1j** formed two hydrogen bonds with Asn260 and Met280 using its two hydroxyls and interacted hydrophobically with Val248, Val283, and Ala286 through its two phenyl rings. On the other hand, compound **1j** interacted hydrophobically with Val 248, Met257, Phe264, Val283, and Ala 286 and by π-π stacking interacted with His263. These LigandScout results agreed well with AutoDock 4 binding affinity results. Summarized, the observations

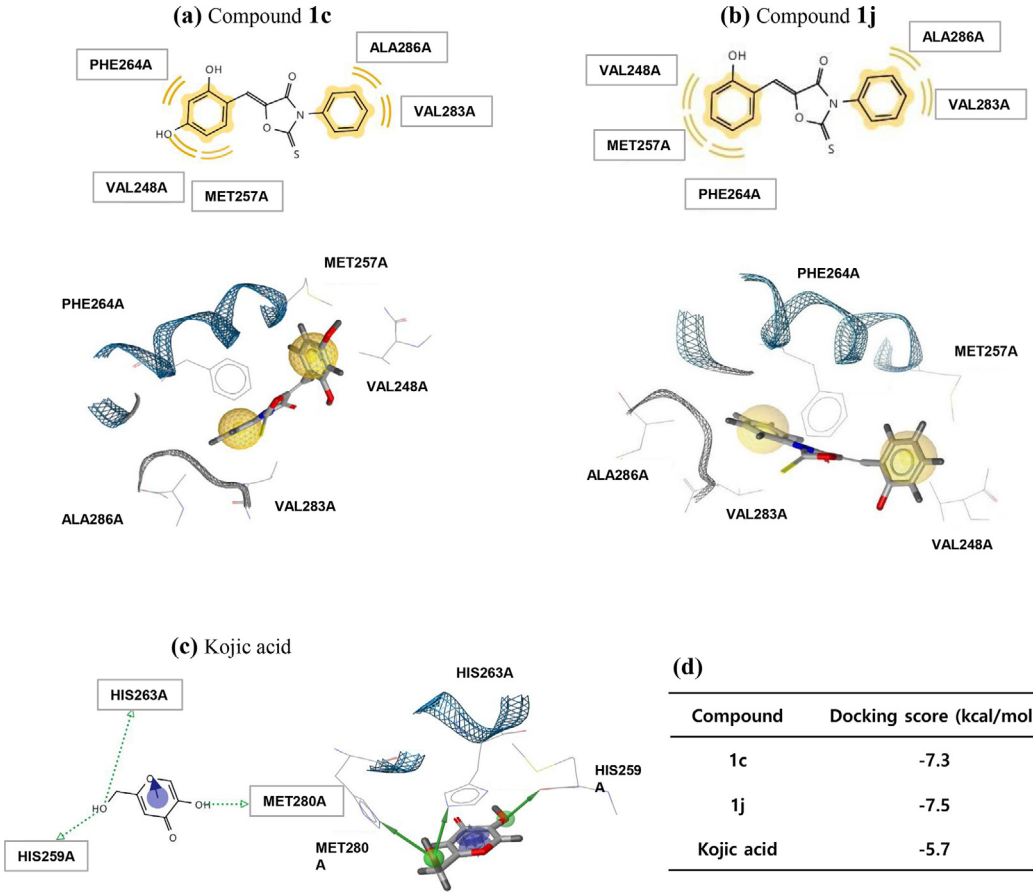

(d)

Compound	Docking score (kcal/mol)
1c	-7.3
1j	-7.5
Kojic acid	-5.7

Fig. 4. Docking simulation of the (*Z*)-5-(substituted benzylidene)-3-phenyl-2-thioxooxazolidin-4-one derivatives **1c** and **1j** and of kojic acid with *Agaricus bisporus* tyrosinase using AutoDock Vina and pharmacophore analysis. (a-c) Pharmacophore results for **1c**, **1j**, and kojic acid obtained using LigandScout 4.3 showed possible hydrophobic (yellow), π-π stacking (violet arrow), and hydrogen bonding (green arrow) interactions between tyrosinase amino acid residues and the three ligands. Docking simulation 3D-results indicated hydrophobic (yellow sphere), π-π stacking (violet ring), and hydrogen bonding (green sphere) regions on the ligands. (d) Docking scores for interactions between tyrosinase and **1c**, **1j**, and kojic acid (PDB code: 2Y9X). (For interpretation of the references to color in this figure legend, the reader is referred to the web version of this article.)

above indicate that the resorcinol (2,4-dihydroxyphenyl) moiety plays an important role in ligand binding to the active site of tyrosinase by forming two hydrogen bonds and participating in two hydrophobic interactions.

Another docking software Schrödinger suite was used to further improve our understanding of the tyrosinase binding interactions of **1c**, **1j** and kojic acid. The binding interactions of kojic acid, **1c** and **1j** are shown in 2D and 3D structures in Fig. 5c. Kojic acid was found to form one hydrogen bond with Gly281 and a π-π stacking with His263. Compound **1c** formed metal coordination and salt bridges with Cu400 and Cu401 and its 2,4-dihydroxyphenyl ring interacted with His259 and His263 by π-π stacking. Compound **1j** formed one hydrogen bond with Asn260 and interacted with His263 by π-π stacking. As can be seen in Fig. 6b, the docking scores obtained by the Schrödinger suite indicated that **1c** more strongly inhibited mushroom tyrosinase than kojic acid and **1j**, which may be due to the metal coordination and salt bridges of **1c** with copper ions.

*2.5. Human tyrosinase homology model for the study of docking simulations of compounds **1c** and **1j** and kojic acid*

To further validate the nature and mode of binding interactions of compound **1c** and **1j** in human tyrosinase, a homology model based on human tyrosinase related protein 1 (TRP1) was used. The entire sequence of human tyrosinase (P14679) was imported from the UniProt database [56] to build the 3D homology model of human tyrosinase. The X-ray structure of TRP1 (PDB ID:5M8Q) [57] was used as a protein template due to its 45.81% sequence identity with the human tyrosinase. The co-crystal ligand and zinc ions were reflected in the newly constructed homology model of human tyrosinase. The 3D structure of the newly constructed human tyrosinase homology model was further prepared using Schrödinger suite and docked to compounds **1c** and **1j** and kojic acid. The homology model of the newly constructed human tyrosinase and the aligned protein sequence are shown in Figure S53.

*2.6. Docking score and binding mode of compounds **1c** and **1j** and kojic acid at the active site of human tyrosinase homology model*

The binding mode of **1c**, **1j** and kojic acid was predicted based on the nature of the binding interactions with amino acids in the active site of the human tyrosinase homology model using Schrödinger suite (Fig. 6a). Kojic acid formed a hydrogen bond with Ser375 and interacted with His367 through π-π stacking. In addition, kojic acid produced a metal coordination with one of the two zinc ions (Zn7). The binding affinity of kojic acid to human tyrosinase was measured with a docking score of −4.15 kcal/mol (Fig. 6b), which was weaker than that of mushroom tyrosinase (−4.65 kcal/mol). Compound **1c** was observed to generate metal coordination and salt bridges with zinc ions (Zn6 and Zn7) in the same way that **1c** interacted with mushroom tyrosinase.

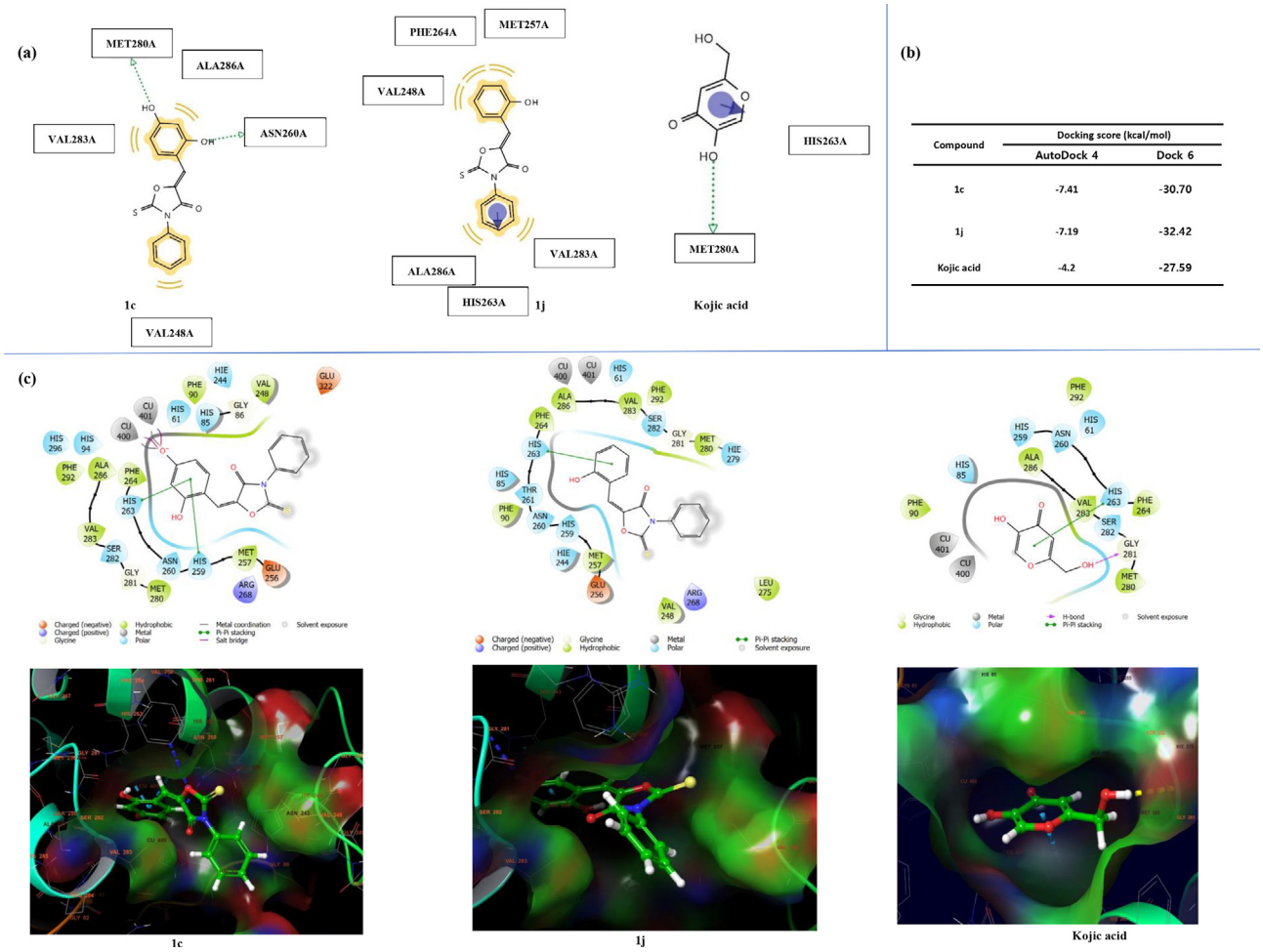

Compound	Docking score (kcal/mol)	
	AutoDock 4	Dock 6
1c	-7.41	-30.70
1j	-7.19	-32.42
Kojic acid	-4.2	-27.59

Fig. 5. Docking simulation of the (Z)-5-(substituted benzylidene)-3-phenyl-2-thioxooxazolidin-4-one derivatives **1c**, and **1j** and of kojic acid with Agaricus bisporus tyrosinase using AutoDock 4, Dock 6 and Schrödinger suite and pharmacophore analysis. (a) Pharmacophore results for **1c**, **1j**, and kojic acid obtained using LigandScout 4.3 based on AutoDock 4 showed possible hydrophobic (yellow), π-π stacking (violet arrow), and hydrogen bonding (green arrow) interactions between tyrosinase amino acid residues and the three ligands. (b) Docking scores for tyrosinase interactions with **1c**, **1j**, and kojic acid (PDB code: 2Y9X). (c) Binding interactions between mushroom tyrosinase and **1c**, **1j**, and kojic acid obtained by Schrödinger suite. (For interpretation of the references to color in this figure legend, the reader is referred to the web version of this article.)

Compound **1c** also interacted with His367 through π-π staking. The combined effect of these interactions on **1c** resulted in a docking score of −5.36 kcal/mol, indicating a stronger binding affinity than kojic acid. However, the binding affinity of **1c** was slightly weaker in human tyrosinase than in mushroom tyrosinase (−5.65 kcal/mol). On the other hand, compound **1j** did not interact with zinc ions, but created a salt bridge with Lys306 and interacted with His202 through π-π staking. In addition, **1j** formed a hydrogen bond with Val377. The calculated docking score for **1j** is −4.57 kcal/mol in human tyrosinase. These docking results imply that both compounds **1c** and **1j** may effectively inhibit mushroom tyrosinase as well as human tyrosinase.

*2.7. Binding analysis of **1c**, **1j** and kojic acid in human tyrosinase homology model and mushroom tyrosinase enzyme*

To compare the interactions of compounds **1c**, **1j** and kojic acid, we performed docking studies using Schrödinger suite on both the human tyrosinase homology model and mushroom tyrosinase and found interesting results. As shown in Figure S54, the distance between the two copper ions and the hydroxyl group of kojic acid in mushroom tyrosinase is 3.14 Å and 3.07 Å, and the distance between the zinc ions and the hydroxyl group of kojic acid in human tyrosinase is 2.55 Å and 2.13 Å. However, the hydroxyl groups of kojic acid that interacted with the metal (Cu or Zn) were different in the two tyrosinases. In mushroom tyrosinase, the phenolic hydroxyl group participated in metal coordination and salt bridges, whereas in human tyrosinase, the alcoholic hydroxyl group was involved in these interactions. The hydrogen bond length of kojic acid was 2.13 Å in mushroom tyrosinase and 1.75 Å in human tyrosinase model. Similarly, the distances between the metal ions (Cu or Zn) and the 4-hydroxyl group of **1c** were recorded as 2.31 Å and 2.35 Å in the mushroom tyrosinase and 2.12 Å and 2.48 Å in the human tyrosinase model, respectively. The distance between the hydroxyl group of **1j** and the copper ions in mushroom tyrosinase was recorded as 5.23 Å and 4.49 Å, indicating the absence of metal coordination and salt bridges between the metal ions and the hydroxyl group. Interestingly, in human tyrosinase, **1j** was located at the active site in a different arrangement from that in mushroom tyrosinase. Unlike in mushroom tyrosinase, the 2-hydroxyphenyl ring of **1j** was far from the zinc ions in human tyrosinase. Instead, the *N*-phenyl ring of **1j** was placed close to the zinc ions with 3.72 Å and 3.30 Å away. The order of decreasing binding affinity for human tyrosinase was **1c**, **1j** and kojic acid, and **1c**, kojic acid and **1j** for mushroom tyrosinase. Regardless of the type of tyrosinase, **1c** showed the strongest

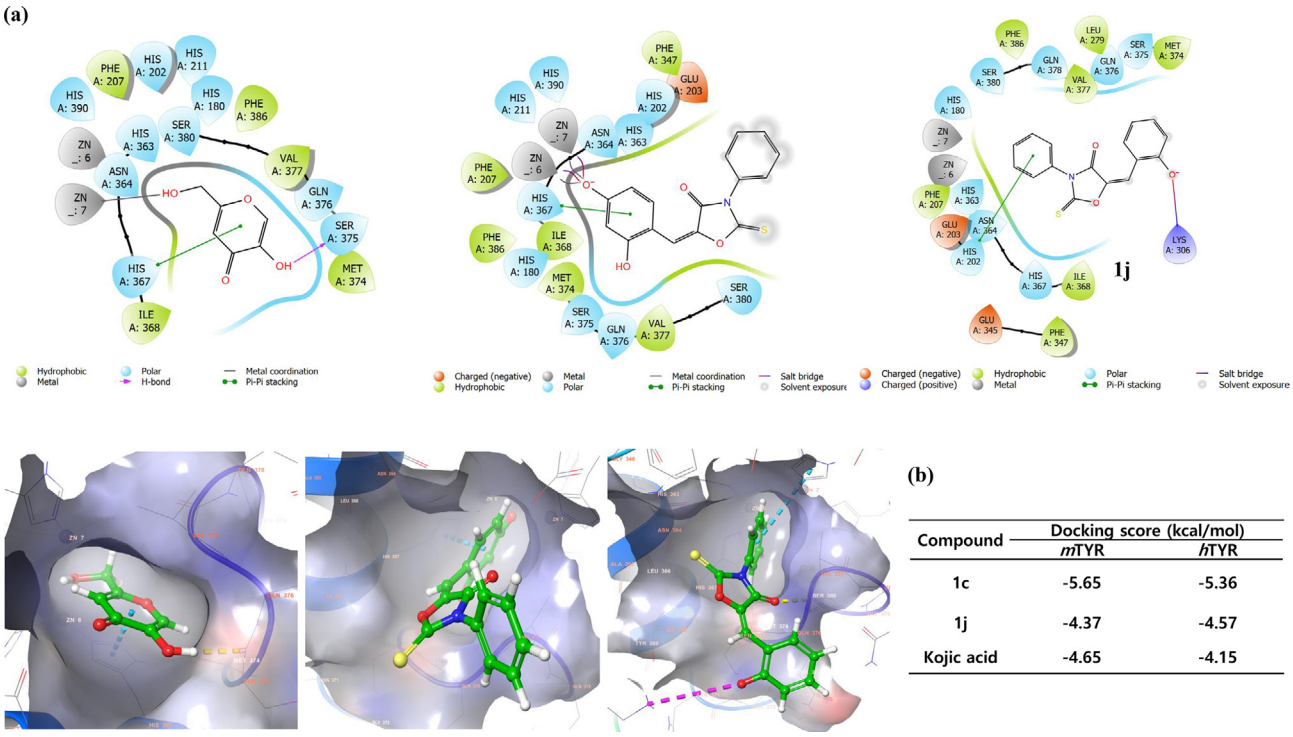

Compound	Docking score (kcal/mol)	
	*m*TYR	*h*TYR
1c	-5.65	-5.36
1j	-4.37	-4.57
Kojic acid	-4.65	-4.15

Fig. 6. Predicted binding mode of **1c**, **1j** and kojic acid at the active site of human tyrosinase homology model and docking score using Schrödinger suite. (a) Pharmacophore results are represented in 2D and 3D structures. (b) Docking scores of **1c**, **1j** and kojic acid using mushroom tyrosinase (PDB: 2Y9X) and human tyrosinase homology model are represented, respectively.

binding affinity to tyrosinase. Although compound **1j** showed lower binding affinity than kojic acid in mushroom tyrosinase docking simulations using Schrödinger suite, results obtained with other docking programs such as AutoDock Vina, AutoDock 4 and Dock 6 indicated that **1j** had a higher binding affinity than kojic acid. These results imply that compounds **1c** and **1j** may effectively inhibit both mushroom tyrosinase and human tyrosinase.

*2.8. Cytotoxic effects of **1c** and **1j** in B16F10 melanoma cells*

An EZ-cytox assay was used to investigate the cytotoxic effects of compounds **1c** and **1j**. After murine B16F10 melanoma cells had been cultured for 24 h, they were treated with different concentrations (0, 5, 10, or 20 μM) of **1c** and **1j** for 24 h in a humidified atmosphere. Optical densities were measured on a microplate reader.

Cell viability results are shown in Figure S55. Compounds **1c** and **1j** did not have a significant cytotoxic effect on B16F10 melanoma cells at concentrations up to 20 μM, which indicated both compounds were non-toxic to these cells at concentrations below 20 μM. Thus, cell-based assays on cellular tyrosinase inhibition and melanin production were performed using **1c** and **1j** at concentrations of $\leq$ 20 μM.

*2.9. Cellular tyrosinase inhibitory activities of compounds **1c** and **1j** in α-MSH- and IBMX-co-stimulated B16F10 melanoma cells*

Cellular tyrosinase inhibitory effect of compounds **1c** and **1j** was investigated by using murine B16F10 melanoma cells co-stimulated with 3-isobutyl-1-methylxanthine (IBMX) and α-melanocyte-stimulating hormone (α-MSH). B16F10 melanoma cells were cultured for 24 h and then pretreated with 20 μM of kojic acid or compounds **1c** or **1j** at concentrations of 0, 5, 10, or 20 μM for 3 h. Cells were then co-treated with α-MSH 1 μM and IBMX 200 μM for 48 h to increase tyrosinase activity. Tyrosinase-inhibitory effects were accessed by measuring optical densities using a microplate reader.

α-MSH and IBMX co-treatment increased cellular tyrosinase activity level 2.65-fold (Fig. 7). Treatments with **1c** or **1j** significantly and concentration-dependently decreased cellular tyrosinase activity enhanced by α-MSH and IBMX co-treatment. Compound **1c** at 10 μM and compound **1j** at 5 μM both inhibited cellular tyrosinase more than kojic acid at 20 μM, and **1j** at 20 μM resulted in cellular tyrosinase activity similar to that of the control group. Considering that **1c** and **1j** had no observable cytotoxic effect at concentrations below 20 μM (Figure S55), these tyrosinase-inhibitory activities were attributed to direct tyrosinase inhibition by **1c** and **1j**. This notion was supported by our docking simulation finding that **1c** and **1j** bind strongly to the active site of tyrosinase.

*2.10. Inhibitory effects of compounds **1c** and **1j** on melanin production in α-MSH and IBMX co-stimulated B16F10 melanoma cells*

Melanin assays were conducted on α-MSH and IBMX co-stimulated B16F10 melanoma cells to investigate the inhibitory effects of compounds **1c** and **1j** on melanin production. Murine B16F10 melanoma cells were seeded in 6-well culture plates and pretreated with 20 μM of kojic acid or compounds **1c** or **1j** at 0, 5, 10, or 20 μM for 3 h. Cells were then co-treated with α-MSH and IBMX for 48 h to increase melanin contents. The inhibitory effects of **1c**, **1j**, and kojic acid on melanin production were determined by measuring optical densities using a microplate reader.

The effects of **1c**, **1j**, and kojic acid on melanin production are shown in Fig. 8. Compounds **1c** and **1j** significantly and potently decreased melanin contents in α-MSH and IBMX co-stimulated B16F10 melanoma cells in a concentration-dependent manner. Interestingly, **1c** at 10 μM and **1j** at 5 μM inhibited melanin production more than kojic acid at 20 μM. These results indicate that

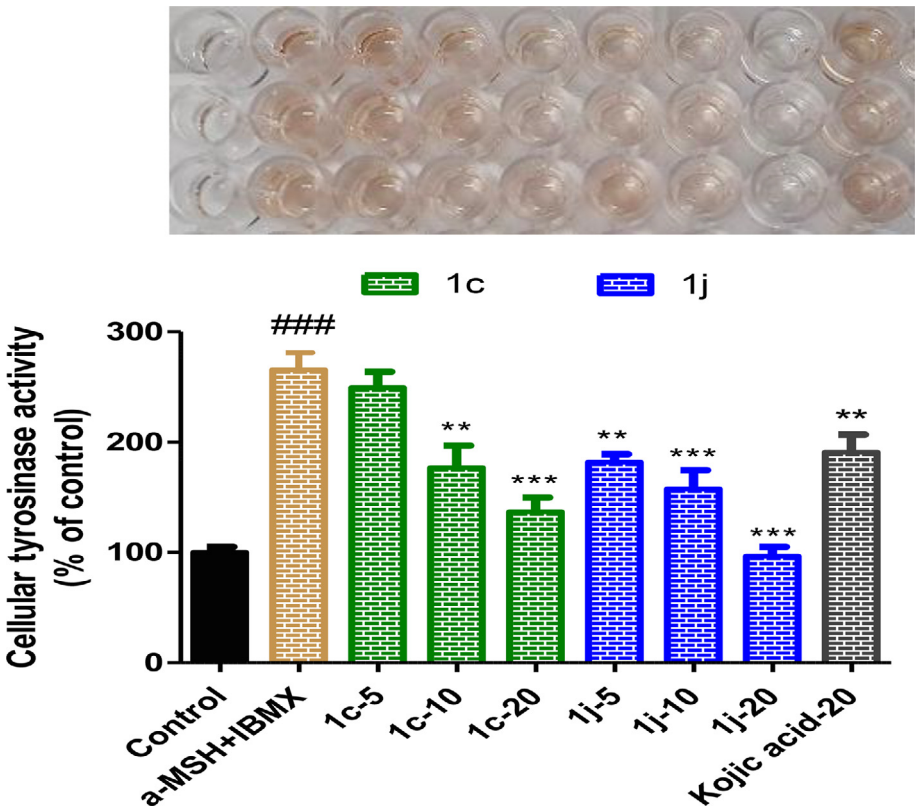

Fig. 7. Cellular tyrosinase inhibitory activities of **1c** and **1j** on murine B16F10 cells. In the presence of 1 μM α-MSH and 200 μM IBMX, B16F10 cells were treated with different concentrations (0, 5, 10, and 20 μM) of **1c**, **1j**, or kojic acid (20 μM) for 24 h. Results are percentages of untreated controls, and columns represent the means ± SEMs of three determinations. $^{###}p < 0.001$ versus untreated controls; $^{**}p < 0.01$, $^{***}p < 0.001$ versus α-MSH and IBMX co-treated cells.

these suppressions of melanin production were mainly caused by the inhibition of tyrosinase activity (Figs. 7 and 8).

3. Conclusion

In summary, sixteen (*Z*)-5-(substituted benzylidene)-3-phenyl-2-thioxooxazolidin-4-one analogues **1a**–**1p** containing the β-phenyl-α,β-unsaturated carbonyl scaffold, which has been reported to play an important role in conferring tyrosinase inhibitory activity, were synthesized by reacting 3-phenyl-2-thioxooxazolidin-4-one (**2**) with different benzaldehydes. Configurations of the exocyclic double bond of synthesized products were determined using C,H-spin-coupling constants. The inhibitory activities of the synthesized compounds against mushroom tyrosinase were evaluated at 25 μM. Of the sixteen compounds, compounds **1c** (78% inhibition) and **1j** (71% inhibition) were found to be more potent than kojic acid (58% inhibition, the positive control). Compounds **1c** and **1j** also had lower IC_{50} values than kojic acid (4.70 ± 0.40 and 11.18 ± 0.54 μM, respectively, *vs.* 23.18 ± 0.11 μM). Lineweaver-Burk plots showed **1c** and **1j** were competitive inhibitors of tyrosinase. Docking simulations of **1c** or **1j** with mushroom tyrosinase were performed using AutoDock Vina, AutoDock 4, Dock 6, and Schrödinger suite. All docking simulations confirmed that compounds **1c** and **1j** bind to the active site of tyrosinase more strongly than kojic acid. Pharmacophore analysis using LigandScout and Schrödinger suite confirmed that the 2,4-dihydroxyphenyl moiety of **1c** formed two hydrogen bonds with the amino acids of tyrosinase at the active site, or metal coordination and salt bridges with the copper ions. Docking simulation results with the human tyrosinase homology model obtained using Schrödinger suite supported the possibility that **1c** and **1j** might strongly inhibit human tyrosinase. Our investigation of the tyrosinase activity and melanin production in α-MSH and IBMX co-stimulated murine B16F10 melanoma cells revealed that **1c** and **1j** effectively inhibited tyrosinase activity and melanogenesis concentration-dependently and more potently than kojic acid without evidence of cytotoxicity. The similarity between the inhibitions of cellular tyrosinase activity and melanin production by **1c** and **1j** suggests their anti-melanogenic effects are the result of tyrosinase inhibition. Furthermore, the observed anti-melanogenic effects of **1c** and **1j** demonstrate these agents have promising potential as skin-lightening therapeutics for the treatment of hyperpigmentation diseases.

4. Experimental section

4.1. General methods

All chemicals and reagents were obtained commercially (Sigma-Aldrich and Alfa Aesar) and used without further purification, and all anhydrous solvents were distilled over CaH_2 or Na/benzophenone before use. Reactions were monitored by thin-layer chromatography (TLC) on glass plates coated with silica gel using a fluorescent indicator (TLC Silica Gel 60 F254, Merck, Germany) and column chromatography was conducted on MP Silica 40–63, 60 Å. High resolution mass spectroscopy data was obtained on an Agilent Accurate Mass Q-TOF (quadruple-time of flight) liquid chromatography mass spectrometer (Agilent, Santa Clara, CA, USA) in negative ESI mode. Low-resolution mass data were obtained in ESI negative or positive mode on an Expression CMS spectrometer (Advion Ithaca, NY, USA). Nuclear magnetic resonance (NMR) spectra were recorded on a Varian Unity INOVA 400 spectrometer or a Varian Unity AS500 spectrometer (Agilent

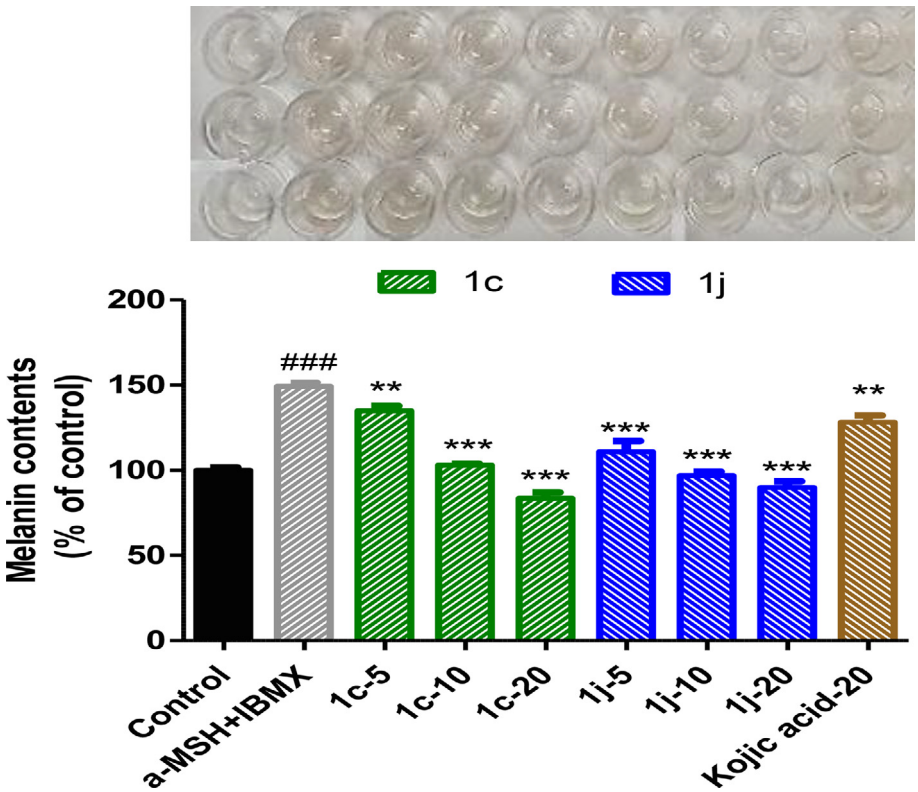

Fig. 8. Effect of compounds **1c** and **1j** on melanogenesis in murine B16F10 cells in the presence of 1 μM α-MSH and 200 μM IBMX. B16F10 cells were treated with varying concentrations (0, 5, 10, and 20 μM) of **1c** and **1j** or kojic acid (20 μM) for 48 h in the presence of α-MSH and IBMX. Melanin contents were measured at 405 nm and columns represent the means ± SEMs of three experiments. Results are expressed as percentages of untreated controls. $^{###}p < 0.001$, versus untreated controls; $^{**}p < 0.01$, $^{***}p < 0.001$ versus cell co-treated with α-MSH and IBMX.

Technologies, Santa Clara, CA, USA) at 400 MHz and 500 MHz ^{1}H NMR, respectively, and on a Varian Unity INOVA 400 spectrometer for 100 MHz ^{13}C NMR. DMSO d_6 (δ_H 2.50 ppm and δ_C 39.7 ppm) or $CDCl_3$ (δ_H 7.24 ppm and δ_C 77.0 ppm) was used as solvents for NMR samples. Coupling constants (*J*) and chemical shifts were measured in hertz (Hz) and parts per million (ppm), respectively. The abbreviations used for ^{1}H NMR data are; s (singlet), d (doublet), t (triplet), q (quartet), dd (doublet of doublets), td (triplet of doublets), m (multiplet), and brs (broad singlet).

*4.1.1. General procedure used for the synthesis of (Z)-5-(substituted benzylidene)-3-phenyl-2-thioxooxazolidin-4-one analogues (**1a–1p**)*

Trimethylamine (1.03 mL, 7.39 mmol) and phenyl isothiocyanate (1.76 mL, 14.74 mmol) were added slowly to a stirred solution of ethyl glycolate (1.4 mL, 14.79 mmol) in dichloromethane (20 mL) at 0 ℃. The reaction mixture was stirred at ambient temperature for 42 h and partitioned between dichloromethane and water. The organic layer was dried over anhydrous $MgSO_4$, filtered, and evaporated *in vacuo*. The resultant residue was purified by silica gel column chromatography using hexane and ethyl acetate (5:1) as eluant to give 3-phenyl-2-thioxooxazolidin-4-one (**2**, 834.7 mg, 29.3%). A solution of **2** (100 mg, 0.52 mmol), a benzaldehyde (1.0 equiv.), and sodium acetate (139 mg, 1.69 mmol) in acetic acid (1.0 mL) was refluxed for 9–25 h. After cooling, water was added to the reaction mixture and the mixture was stirred for 1 h. The precipitate generated was filtered and washed with water to give (*Z*)-5-(substituted benzylidene)-3-phenyl-2-thioxoox azolidin-4-one derivatives (**1a–1p**) as solids in yields of 18–85%.

*4.1.1.1. 3-Phenyl-2-thioxooxazolidin-4-one (**2**).* ^{1}H NMR (400 MHz, $CDCl_3$) δ 7.53–7.46 (m, 3H, 3-H, 4-H, 5-H), 7.29 (d, 2H, *J* = 8.4 Hz, 2-H, 6-H), 4.97 (s, 2H, CH_2); ^{13}C NMR (100 MHz, $CDCl_3$) δ 190.2, 170.5, 132.2, 130.1, 129.8, 127.7, 70.5.

*4.1.1.2. (Z)-5-(4-Hydroxybenzylidene)-3-phenyl-2-thioxooxazolidin-4-one (**1a**).* Yellow solid; reaction time, 22 h, yield, 52%; ^{1}H NMR (500 MHz, DMSO d_6) δ 10.34 (brs, 1H, OH), 7.79 (d, 2H, *J* = 9.0 Hz, 2′-H, 6′-H), 7.54 (t, 2H, *J* = 7.0 Hz, 3-H, 5-H), 7.49 (t, 1H, *J* = 7.0 Hz, 4-H), 7.46 (d, 2H, *J* = 7.5 Hz, 2-H, 6-H), 6.92 (s, 1H, vinylic H), 6.92 (d, 2H, *J* = 9.0 Hz, 3′-H, 5′-H); ^{13}C NMR (100 MHz, DMSO d_6) δ 183.8, 162.1, 160.9, 137.9, 134.2, 133.5, 130.1, 129.8, 128.7, 122.7, 117.0, 114.5; LRMS (ESI-) *m*/*z* 296 $(M-H)^-$.

*4.1.1.3. (Z)-5-(3,4-Dihydroxybenzylidene)-3-phenyl-2-thioxooxazolidin-4-one (**1b**).* Green solid; reaction time, 10 h, yield, 70%; ^{1}H NMR (500 MHz, DMSO d_6) δ 9.84 (s, 1H, OH), 9.49 (s, 1H, OH), 7.53 (t, 2H, *J* = 7.5 Hz, 3-H, 5-H), 7.48 (t, 1H, *J* = 7.0 Hz, 4-H), 7.46–7.44 (m, 3H, 2-H, 6-H, 2′-H), 7.22 (d, 1H, *J* = 7.5 Hz, 6′-H), 6.85 (d, 1H, *J* = 8.0 Hz, 5′-H), 6.82 (s, 1H, vinylic H); ^{13}C NMR (100 MHz, DMSO d_6) δ 183.8, 162.1, 149.9, 146.5, 137.7, 133.5, 130.1, 129.8, 128.7, 125.9, 123.1, 118.3, 116.8, 115.1; LRMS (ESI-) *m*/*z* 312 $(M-H)^-$.

*4.1.1.4. (Z)-5-(2,4-Dihydroxybenzylidene)-3-phenyl-2-thioxooxazolidin-4-one (**1c**).* Brown solid; reaction time, 22 h, 18%; ^{1}H NMR (500 MHz, DMSO d_6) δ 10.52 (s, 1H, OH), 10.25 (s, 1H, OH), 7.82 (d, 1H, *J* = 8.5 Hz, 6′-H), 7.53 (t, 2H, *J* = 7.5 Hz, 3-H, 5-H), 7.48 (t, 1H, *J* = 7.0 Hz, 4-H), 7.45 (d, 2H, *J* = 7.0 Hz, 2-H, 6-H), 7.05 (s, 1H, vinylic H), 6.45 (dd, 1H, *J* = 8.0, 2.0 Hz, 5′-H), 6.41 (d, 1H, *J* = 2.0 Hz, 3′-H); ^{13}C NMR (100 MHz, DMSO d_6) δ 183.6, 162.8, 162.1, 160.2, 136.9, 133.5, 132.8, 130.1, 129.8, 128.7, 110.3, 109.6, 109.0, 103.0; LRMS (ESI-) *m*/*z* 312 $(M-H)^-$; HRMS (ESI +) *m*/*z* $C_{16}H_{12}NO_4S$ $(M + H)^+$ calcd 314.0482, obsd 314.0483, *m*/*z* $C_{16}H_{11}NNaO_4S$ $(M + Na)^+$ calcd 336.0301, obsd 336.0304.

*4.1.1.5. (Z)-5-(4-Hydroxy-3-methoxybenzylidene)-3-phenyl-2-thioxooxazolidin-4-one (**1d**).* Yellow solid; reaction time, 21 h, 18%; ^{1}H

NMR (500 MHz, $CDCl_3$) δ 7.55 (t, 2H, J = 7.5 Hz, 3-H, 5-H), 7.50 (t, 1H, J = 7.0 Hz, 4-H), 7.47 (s, 1H, 2′-H), 7.41–7.39 (m, 3H, 2-H, 6-H, 6′-H), 7.00 (d, 1H, J = 8.5 Hz, 5′-H), 6.78 (s, 1H, vinylic H), 6.06 (s, 1H, OH), 3.98 (s, 3H, OCH_3); ^{13}C NMR (100 MHz, $CDCl_3$) δ 182.4, 161.8, 149.1, 147.1, 137.5, 132.5, 129.9, 129.6, 127.6, 127.3, 123.6, 115.5, 115.4, 113.2, 56.3; LRMS (ESI-) m/z 326 $(M-H)^-$, 311 $(M-H-CH_3)^-$.

*4.1.1.6. (Z)-5-(3-Ethoxy-4-hydroxybenzylidene)-3-phenyl-2-thioxooxazolidin-4-one (**1e**).* Green solid; reaction time, 22 h, 55%; ^{1}H NMR (500 MHz, DMSO d_6) δ 9.91 (s, 1H, OH), 7.53 (t, 2H, J = 7.0 Hz, 3-H, 5-H), 7.50–7.43 (m, 5H, 2-H, 4-H, 6-H, 2′-H, 6′-H), 6.94 (d, 1H, J = 8.0 Hz, 5′-H), 6.90 (s, 1H, vinylic H), 4.05 (q, 2H, J = 6.5 Hz, OCH_2-CH_3), 1.34 (t, 3H, J = 6.5 Hz, OCH_2CH_3); ^{13}C NMR (100 MHz, DMSO d_6) δ 183.7, 162.1, 150.9, 147.7, 137.9, 133.4, 130.1, 129.8, 128.7, 126.5, 123.1, 117.2, 117.1, 114.8, 64.7, 15.3; LRMS (ESI-) m/z 340 $(M-H)^-$, 311 $(M-H-C_2H_5)^-$.

*4.1.1.7. (Z)-5-(3-Hydroxy-4-methoxybenzylidene)-3-phenyl-2-thioxooxazolidin-4-one (**1f**).* Yellow solid; reaction time, 21 h, 85%; ^{1}H NMR (500 MHz, $CDCl_3$) δ 7.55 (t, 2H, J = 7.5 Hz, 3-H, 5-H), 7.52 (s, 1H, 2′-H), 7.49 (t, 1H, J = 7.5 Hz, 4-H), 7.42 (d, 1H, J = 8.5 Hz, 6′-H), 7.39 (d, 2H, J = 7.0 Hz, 2-H, 6-H), 6.93 (d, 1H, J = 8.5 Hz, 5′-H), 6.76 (s, 1H, vinylic H), 5.68 (s, 1H, OH), 3.97 (s, 3H, OCH_3); ^{13}C NMR (100 MHz, $CDCl_3$) δ 182.5, 161.9, 149.4, 146.2, 137.9, 132.6, 129.9, 129.6, 127.6, 125.6, 124.5, 117.3, 115.1, 111.1, 56.3; LRMS (ESI-) m/z 326 $(M-H)^-$, 311 $(M-H-CH_3)^-$.

*4.1.1.8. (Z)-5-(4-Methoxybenzylidene)-3-phenyl-2-thioxooxazolidin-4-one (**1g**).* Yellow solid; reaction time, 21 h, 68%; ^{1}H NMR (500 MHz, $CDCl_3$) δ 7.85 (d, 2H, J = 8.5 Hz, 2′-H, 6′-H), 7.55 (t, 2H, J = 7.5 Hz, 3-H, 5-H), 7.50 (t, 1H, J = 7.5 Hz, 4-H), 7.40 (d, 2H, J = 7.0 Hz, 2-H, 6-H), 6.99 (d, 2H, J = 8.5 Hz, 3′-H, 5′-H), 6.81 (s, 1H, vinylic H), 3.88 (s, 3H, OCH_3); ^{13}C NMR (100 MHz, $CDCl_3$) δ 182.5, 162.2, 161.9, 137.6, 133.8, 132.6, 129.9, 129.6, 127.6, 123.7, 115.1, 115.0, 55.7; HRMS (ESI +) m/z $C_{17}H_{14}NO_3S$ $(M+H)^+$ calcd 312.0689, obsd 312.0686.

*4.1.1.9. (Z)-5-(2,4-Dimethoxybenzylidene)-3-phenyl-2-thioxooxazolidin-4-one (**1h**).* Yellow solid; reaction time, 16 h, 65%; ^{1}H NMR (500 MHz, DMSO d_6) δ 7.97 (d, 1H, J = 9.0 Hz, 6′-H), 7.54 (t, 2H, J = 7.0 Hz, 3-H, 5-H), 7.49 (t, 1H, J = 7.0 Hz, 4-H), 7.45 (d, 2H, J = 7.5 Hz, 2-H, 6-H), 7.01 (s, 1H, vinylic H), 6.78 (dd, 1H, J = 9.0, 1.5 Hz, 5′-H), 6.69 (d, 1H, J = 1.5 Hz, 3′-H), 3.90 (s, 3H, OCH_3), 3.85 (s, 3H, OCH_3); ^{13}C NMR (100 MHz, DMSO d_6) δ 183.7, 164.0, 162.2, 160.7, 138.3, 133.4, 132.7, 130.1, 129.8, 128.7, 112.8, 108.0, 107.2, 99.1, 56.8, 56.4; HRMS (ESI +) m/z $C_{18}H_{16}NO_4S$ $(M+H)^+$ calcd 342.0795, obsd 342.0796.

*4.1.1.10. (Z)-5-(3,4-Dimethoxybenzylidene)-3-phenyl-2-thioxooxazolidin-4-one (**1i**).* Yellow solid; reaction time, 12 h, 58%; ^{1}H NMR (500 MHz, DMSO d_6) δ 7.58–7.53 (m, 4H, 3-H, 5-H, 2′-H, 6′-H), 7.49 (t, 1H, J = 7.0 Hz, 4-H), 7.46 (d, 2H, J = 7.0 Hz, 2-H, 6-H), 7.15 (d, 1H, J = 8.5 Hz, 5′-H), 6.95 (s, 1H, vinylic H), 3.83 (s, 3H, OCH_3), 3.79 (s, 3H, OCH_3); ^{13}C NMR (100 MHz, DMSO d_6) δ 183.7, 162.1, 152.0, 149.5, 138.6, 133.4, 130.1, 129.8, 128.7, 126.1, 124.4, 115.0, 114.1, 113.0, 56.4, 56.3; HRMS (ESI +) m/z $C_{18}H_{16}NO_4S$ $(M+H)^+$ calcd 342.0795, obsd 342.0796, m/z $C_{18}H_{15}NNaO_4S$ $(M+Na)^+$ calcd 364.0614, obsd 364.0624.

*4.1.1.11. (Z)-5-(2-Hydroxybenzylidene)-3-phenyl-2-thioxooxazolidin-4-one (**1j**).* Green solid; reaction time, 25 h, 28%; ^{1}H NMR (500 MHz, DMSO d_6) δ 10.55 (s, 1H, OH), 7.94 (d, 1H, J = 8.0 Hz, 6′-H), 7.54 (t, 2H, J = 7.0 Hz, 3-H, 5-H), 7.49 (t, 1H, J = 7.0 Hz, 4-H), 7.47 (d, 2H, J = 7.5 Hz, 2-H, 6-H), 7.32 (t, 1H, J = 7.5 Hz, 4′-H), 7.10 (s, 1H, vinylic H), 6.98 (t, 1H, J = 7.5 Hz, 5′-H), 6.97 (d, 1H, J = 7.5 Hz, 3′-H); ^{13}C NMR (100 MHz, DMSO d_6) δ 183.9, 162.2, 158.0, 139.3, 133.4, 133.2, 131.2, 130.2, 129.8, 128.7, 120.6, 118.5, 116.7, 107.5; HRMS (ESI +) m/z $C_{16}H_{12}NO_3S$ $(M+H)^+$ calcd 298.0532, obsd 298.0537, m/z $C_{16}H_{11}NNaO_3S$ $(M+Na)^+$ calcd 320.0352, obsd 320.0362.

*4.1.1.12. (Z)-3-Phenyl-2-thioxo-5-(3,4,5-trimethoxybenzylidene)oxazolidin-4-one (**1k**).* Yellow solid; reaction time, 25 h, 64%; ^{1}H NMR (500 MHz, $CDCl_3$) δ 7.55 (t, 2H, J = 7.5 Hz, 3-H, 5-H), 7.50 (t, 1H, J = 7.5 Hz, 4-H), 7.40 (d, 2H, J = 7.5 Hz, 2-H, 6-H), 7.13 (s, 2H, 2′-H, 6′-H), 6.76 (s, 1H, vinylic H), 3.93 (s, 9H, 3XOCH_3); ^{13}C NMR (100 MHz, $CDCl_3$) δ 182.2, 161.8, 153.7, 141.4, 138.4, 132.5, 129.9, 129.7, 127.6, 126.2, 114.9, 109.3, 61.2, 56.5; HRMS (ESI +) m/z $C_{19}H_{18}NO_5S$ $(M+H)^+$ calcd 372.0900, obsd 372.0906, m/z $C_{19}H_{17}NNaO_5S$ $(M+Na)^+$ calcd 394.0720, obsd 394.0722.

*4.1.1.13. (Z)-5-(4-Hydroxy-3,5-dimethoxybenzylidene)-3-phenyl-2-thioxooxazolidin-4-one (**1l**).* Yellow solid; reaction time, 25 h, 54%; ^{1}H NMR (500 MHz, $CDCl_3$) δ 7.55 (t, 2H, J = 7.5 Hz, 3-H, 5-H), 7.50 (t, 1H, J = 7.5 Hz, 4-H), 7.40 (d, 2H, J = 7.0 Hz, 2-H, 6-H), 7.16 (s, 2H, 2′-H, 6′-H), 6.76 (s, 1H, vinylic H), 5.96 (s, 1H, OH), 3.97 (s, 6H, 2XOCH_3); ^{13}C NMR (100 MHz, $CDCl_3$) δ 182.3, 161.8, 147.6, 138.5, 137.7, 132.5, 129.9, 129.7, 127.6, 122.5, 115.5, 109.1, 56.7; LRMS (ESI-) m/z 356 $(M-H)^-$, 341 $(M-H-CH_3)^-$.

*4.1.1.14. (Z)-5-(3,5-Di-tert-butyl-4-hydroxybenzylidene)-3-phenyl-2-thioxooxazolidin-4-one (**1m**).* Yellow solid; reaction time, 20 h, 34%; ^{1}H NMR (400 MHz, $CDCl_3$) δ 7.73 (s, 2H, 2′-H, 6′-H), 7.52 (t, 2H, J = 7.6 Hz, 3-H, 5-H), 7.46 (t, 1H, J = 7.2 Hz, 4-H), 7.37 (d, 2H, J = 7.2 Hz, 2-H, 6-H), 6.80 (s, 1H, vinylic H), 5.71 (s, 1H, OH), 1.46 (s, 18H, 2X*t*-Bu); ^{13}C NMR (100 MHz, $CDCl_3$) δ 182.5, 162.0, 157.2, 137.2, 137.1, 132.7, 129.8, 129.7, 129.6, 127.7, 122.8, 116.6, 34.6, 30.3; LRMS (ESI-) m/z 408 $(M-H)^-$.

*4.1.1.15. (Z)-5-(3-Bromo-4-hydroxybenzylidene)-3-phenyl-2-thioxooxazolidin-4-one (**1n**).* Yellow solid; reaction time, 25 h, 56%; ^{1}H NMR (500 MHz, DMSO d_6) δ 11.17 (s, 1H, OH), 8.08 (d, 1H, J = 1.5 Hz, 2′-H), 7.79 (dd, 1H, J = 8.5, 1.5 Hz, 6′-H), 7.53 (t, 2H, J = 7.5 Hz, 3-H, 5-H), 7.49 (t, 1H, J = 7.0 Hz, 4-H), 7.45 (d, 2H, J = 7.0 Hz, 2-H, 6-H), 7.10 (d, 1H, J = 8.5 Hz, 5′-H), 6.93 (s, 1H, vinylic H); ^{13}C NMR (100 MHz, DMSO d_6) δ 183.7, 162.0, 157.2, 138.7, 136.6, 133.4, 132.8, 130.2, 129.8, 128.7, 124.4, 117.7, 112.6, 110.8; LRMS (ESI-) m/z 374 $(M-H)^-$, 376 $(M+2-H)^-$.

*4.1.1.16. (Z)-5-(3,5-Dibromo-4-hydroxybenzylidene)-3-phenyl-2-thioxooxazolidin-4-one (**1o**).* Yellow solid; reaction time, 20 h, 77%; ^{1}H NMR (500 MHz, DMSO d_6) δ 10.84 (brs, 1H, OH), 8.11 (s, 2H, 2′-H, 6′-H), 7.54 (t, 2H, J = 7.5 Hz, 3-H, 5-H), 7.50 (t, 1H, J = 7.0 Hz, 4-H), 7.45 (d, 2H, J = 7.0 Hz, 2-H, 6-H), 6.94 (s, 1H, vinylic H); ^{13}C NMR (100 MHz, DMSO d_6) δ 183.6, 161.9, 153.5, 139.7, 135.4, 133.3, 130.2, 129.9, 128.6, 126.2, 112.9, 110.5; LRMS (ESI-) m/z 452 $(M-H)^-$, 454 $(M+4-H)^-$, 456 $(M+6-H)^-$.

*4.1.1.17. (Z)-5-(2,4-Difluorobenzylidene)-3-phenyl-2-thioxooxazolidin-4-one (**1p**).* Ivory solid; reaction time, 20 h, 40%; ^{1}H NMR (500 MHz, $CDCl_3$) δ 8.28 (td, 1H, J = 8.0, 6.5 Hz, 6′-H), 7.56 (t, 2H, J = 7.5 Hz, 3-H, 5-H), 7.51 (t, 1H, J = 7.0 Hz, 4-H), 7.39 (d, 2H, J = 7.0 Hz, 2-H, 6-H), 7.08 (s, 1H, vinylic H), 7.07 (td, 1H, J = 8.0, 2.5 Hz, 5′-H), 6.92 (td, 1H, J = 9.5, 2.5 Hz, 3′-H); ^{13}C NMR (100 MHz, $CDCl_3$) δ 182.0, 164.7 (dd, J = 246.2, 32.3 Hz), 162.1 (dd, J = 244.8, 12.0 Hz), 161.4, 139.6, 133.2 (dd, J = 10.0, 2.7 Hz), 132.3, 130.1, 129.7, 127.6, 115.9 (dd, J = 12.3, 4.1 Hz), 113.0 (dd, J = 21.6, 3.7 Hz), 104.8 (dd, J = 15.6, 10.3 Hz), 104.5 (d, J = 25.5 Hz); HRMS (ESI +) m/z $C_{16}H_{10}F_2NO_2S$ $(M+H)^+$ calcd 318.0395, obsd 318.0395.

4.2. Biological evaluation

4.2.1. Mushroom tyrosinase inhibition assay

(*Z*)-5-(Substituted benzylidene)-3-phenyl-2-thioxooxazolidin-4-one derivatives **1a**–**1p** were evaluated for mushroom tyrosinase inhibitory activity as previously described [58]. Briefly, 10 μL of **1a**–**1p** (final concentration: 25 μM), 20 μL of tyrosinase solution, and 170 μL of substrate solution [potassium phosphate buffer 14. 7 mM + 293 μM L-tyrosine solution (1:1, v/v)] were added to a 96-well microplate. The microplate was then wrapped with aluminum foil and incubated for 0.5 h at 37 ^{0}C. Optical densities were measured using a microplate reader (VersaMax^{TM}, Molecular Devices, Sunnyvale, CA, USA) at 475 nm. Kojic acid (25 μM) was used as the positive control. The experiments were performed independently three times. Mushroom tyrosinase inhibitions were calculated using the following equation.

$$\%\text{Inhibition} = [1 - (A/B)] \times 100$$

where A is the absorbance of the test compound and B is the absorbance of the blank.

To determine the IC_{50} values of **1c**, **1j**, and kojic acid, dose-dependent inhibition experiments were carried out in triplicate. Logarithmic percentage inhibitions observed at 3–5 concentrations per experiment were plotted and curve-fitting equations were derived. Individual IC_{50} values were then defined as the concentrations that achieved 50% inhibition.

4.2.2. Kinetic studies of tyrosinase inhibition

Mushroom tyrosinase solution (20 μL, 150 units) and 10 μL of test compounds **1c** or **1j** (final concentrations: 2.5, 5, or 10 μM for **1c** and 5, 10, or 20 μM for **1j**) were added to a 96-well plate containing a mixture (170 μL) consisting of an aqueous solution of L-tyrosine at concentrations of 0.5, 1.0, 2.0, 4.0, or 8.0 mM, 50 mM potassium phosphate buffer (pH 6.5), and distilled water in the ratio 10:10:9. The initial rate of formation of dopachrome in the reaction mixture was determined by measuring increases in absorbance at 475 nm (ΔOD_{475}/min) using a microplate reader. Michaelis constant (K_M) and maximal velocity (V_{max}) of tyrosinase activity were determined using Lineweaver-Burk plots (inverse of reaction velocity (1/V) versus the inverse of substrate concentration (1/[S])) obtained using different concentrations of L-tyrosine. Inhibitory mechanisms were determined using points of convergence of plot lines.

4.2.3. Docking studies of compounds *1c*, and *1j*, and tyrosinase

Binding energies between tyrosinase and compounds **1c** or **1j** or kojic acid were determined as previously reported with slight modification [5,59]. Briefly, Chem3D Pro 12.0 software was used to create 3D structures of the two compounds and the 3D structure of *Agaricus bisporus* tyrosinase was imported from PDB (ID: 2Y9X). Docking scores were calculated using AutoDock Vina 1.1.2, AutoDock 4 [59], Dock 6 [5], and Chimera software. LigandScout 4.3 was used to generate a pharmacophore model to show possible interactions between ligands and amino acid residues of tyrosinase.

4.2.4. Homology model of human tyrosinase and docking studies of compounds *1c*, and *1j*, and tyrosinase

The homology model of human tyrosinase was built using the Swiss-Model online server and the Schrödinger Suite 2020–2 release. The full sequence of human tyrosinase (P14679) was obtained from the UnitPro database, and due to the highest sequence identity with human tyrosinase, the crystal structure of human tyrosinase-related protein 1 (PDB ID: 5M8Q) was used as the protein template. The homology model structure of human tyrosinase was downloaded from the Swiss-Model server and further processed by the Schrödinger suite using the Protein Preparation Wizard. The homologous structure of human tyrosinase has also been validated in Prime, a homology modeling tool from the Schrödinger Suite. The structures of compounds **1c**, and **1j** and kojic were imported to the entry list in CDXML format and prepared for docking using LigPrep [60]. The prepared structures were docked with the homology model using Schrödinger Suite's Ligand Docking Wizard, and 2D and 3D confirmations of the ligand protein complex were prepared [61].

4.2.5. B16F10 cell culture

Murine B16F10 melanoma cells were obtained from the American Type Culture Collection (Manassas, VA, USA) and used for cell viability, cellular tyrosinase activity, and melanin content assays. B16F10 cells were cultured in Dulbecco's modified Eagle's medium containing 10% FBS (fetal bovine serum), and 1% streptomycin at 37 °C in a 5% CO_2 environment, and these cells were then used in cell viability, cellular tyrosinase activity, and melanin content assays in 96-well plates or 6-well dishes. All experiments were independently performed in triplicate.

4.2.6. Cell viability assay: EZ-cytox assay

Cell viability was determined using the EZ-cytox assay. Briefly, B16F10 cells were seeded in a 96-well plate at a density of 5×10^4 cells/well and incubated at 37 °C in a humidified 5% CO_2 environment overnight. Cells were treated with compounds **1c** or **1j** at 0, 5, 10 or 20 μM/well for 24 h, and then EZ-cytox solution (10 μL/well, Daeil Lab Service, Seoul) was added to treated and control cells and incubated at 37 °C for 3 h. Cell viabilities were determined by measuring absorbances at 450 nm using a microplate reader. All experiments were independently performed in triplicate.

4.2.7. Cellular tyrosinase inhibition assays of *1c* and *1j* in B16F10 melanoma cells

Cellular tyrosinase inhibition assays were conducted as previously described with minor changes [62]. Pre-cultured cells were pretreated with compounds **1c** or **1j** at 0, 5, 10, or 20 μM for 3 h. α-MSH and IBMX were then added to final concentrations of 1 μM and 200 μM, respectively, and cells were incubated for 48 h. Cells were then washed with PBS two or three times, lysed with 100 μL of buffer [90 μL of PBS (50 mM), 5 μL of PMSF (0.1 mM), and 5 μL of 1% Triton X-100], and lysates were frozen (−80 °C for 0.5 h) then centrifuged (12,000 rpm for 30 min) at 4 °C. Lysate supernatants (80 μL) in 96-well microplates, were mixed with 20 μL of L-dopa (2 mg/mL) and kept in an incubator at 37 °C for 15 min. Optical densities were measured at 475 nm using a microplate reader (Tecan, Männedorf, Switzerland). All experiments were independently performed in triplicate.

4.2.8. Effects of *1c* and *1j* on melanin contents in B16F10 melanoma cells

The effects of **1c** and **1j** on melanin production in B16F10 cells were evaluated as previously described with minor changes [63]. Briefly, pre-cultured cells were pretreated with **1c** or **1j** at 0, 5, 10 or 20 μM and incubated for 3 h and then 1 μM of α-MSH and 200 μM of IBMX were added. After incubation of 48 h, cells were washed 2 to 3 times with PBS buffer and then incubated in 100 μL of 1 N NaOH for 1 h at 60 °C to dissolve the melanin. Optical densities were measured at 405 nm using a microplate reader to determine melanin contents. All experiments were independently performed in triplicate.

4.2.9. Statistical analysis

The significances of differences between groups were determined by one-way ANOVA and Tukey's test. Graph Pad Prism 5

was used for the analysis and results are expressed as means ± SEMs. Two-sided *P*-values of <0.05 were considered statistically significant.

Declaration of Competing Interest

The authors declare that they have no known competing financial interests or personal relationships that could have appeared to influence the work reported in this paper.

Acknowledgment

This work was supported by a National Research Foundation of Korea (NRF) grant funded by the Korea government (MSIT) (No. NRF-2020R1A2C1004198).

Appendix A. Supplementary data

Supplementary data to this article can be found online at https://doi.org/10.1016/j.csbj.2020.12.001.

References

[1] Ando H, Kondoh H, Ichihashi M, Hearing VJ. Approaches to identify inhibitors of melanin biosynthesis via the quality control of tyrosinase. J Invest Dermatol 2007;127(4):751–61. https://doi.org/10.1038/sj.jid.5700683.
[2] Chedekel MR, Post PW, Deibel RM, Kalus M. Photodestruction of phaeomelanin. Photochem Photobiol 1977;26(6):651–3. https://doi.org/10.1111/j.1751-1097.1977.tb07546.x.
[3] Germain P, Staels B, Dacquet C, Spedding M, Laudet V. Overview of Nomenclature of Nuclear Receptors. Pharmacol Rev 2006;58(4):685–704. https://doi.org/10.1124/pr.58.4.2.
[4] Kumar KJS, Vani MG, Wang S-Y, Liao J-W, Hsu L-S, Yang H-L, Hseu Y-C. In vitro and in vivo studies disclosed the depigmenting effects of gallic acid: A novel skin lightening agent for hyperpigmentary skin diseases. BioFactors 2013;39(3):259–70. https://doi.org/10.1002/biof.1064.
[5] Moustakas DT, Lang PT, Pegg S, Pettersen E, Kuntz ID, Brooijmans N, Rizzo RC. Development and validation of a modular, extensible docking program: DOCK 5. J Comput Aided Mol Des 2006;20(10-11):601–19. https://doi.org/10.1007/s10822-006-9060-4.
[6] Afshin A et al. Health Effects of Overweight and Obesity in 195 Countries over 25 Years. N Engl J Med 2017;377(1):13–27.
[7] tyrosinase retardant. 2013, Google Patents.
[8] Eun Lee K, Bharadwaj S, Yadava U, Gu Kang S. Evaluation of caffeine as inhibitor against collagenase, elastase and tyrosinase using in silico and in vitro approach. J Enzyme Inhib Med Chem 2019;34(1):927–36. https://doi.org/10.1080/14756366.2019.1596904.
[9] Costin G-E, Hearing VJ. Human skin pigmentation: melanocytes modulate skin color in response to stress. FASEB J 2007;21(4):976–94. https://doi.org/10.1096/fj.06-6649rev.
[10] Lu H, Yang Ke, Zhan L, Lu T, Chen X, Cai X, Zhou C, Li He, Qian L, Lv G, Chen S. Optimization of Flavonoid Extraction in Dendrobium officinale Leaves and Their Inhibitory Effects on Tyrosinase Activity. Int J Anal Chem 2019;2019:1–10. https://doi.org/10.1155/2019/7849198.
[11] Chen W-C et al. Discovery of highly potent tyrosinase inhibitor, T1, with significant anti-melanogenesis ability by zebrafish in vivo assay and computational molecular modeling. Sci Rep 2015;5:7995.
[12] Oh E, et al. A Novel Role of Serotonin Receptor 2B Agonist as an Anti-Melanogenesis Agent. Int J Molecular Sci, 2016;17(4):546.
[13] Lee J-Y, Choi H-J, Chung T-W, Kim C-H, Jeong H-S, Ha K-T. Caffeic Acid Phenethyl Ester Inhibits Alpha-Melanocyte Stimulating Hormone-Induced Melanin Synthesis through Suppressing Transactivation Activity of Microphthalmia-Associated Transcription Factor. J Nat Prod 2013;76(8):1399–405. https://doi.org/10.1021/np400129z.
[14] Wang Y et al. Artopithecins A-D, Prenylated 2-Arylbenzofurans from the Twigs of Artocarpus pithecogallus and Their Tyrosinase Inhibitory Activities. Chem Pharm Bull (Tokyo) 2018;66(12):1199–202.
[15] Chu H-L, Wang B-S, Duh P-D. Effects of Selected Organo-sulfur Compounds on Melanin Formation. J Agric Food Chem 2009;57(15):7072–7. https://doi.org/10.1021/jf9005824.
[16] Brotzman N, Xu Y, Graybill A, Cocolas A, Ressler A, Seeram NP, Ma H, Henry GE. Synthesis and tyrosinase inhibitory activities of 4-oxobutanoate derivatives of carvacrol and thymol. Bioorg Med Chem Lett 2019;29(1):56–8. https://doi.org/10.1016/j.bmcl.2018.11.013.
[17] Lee B, Moon KM, Lee B-S, Yang J-H, Park KI, Cho W-K, Ma JY. Swertiajaponin inhibits skin pigmentation by dual mechanisms to suppress tyrosinase. Oncotarget 2017;8(56):95530–41. https://doi.org/10.18632/oncotarget.20913.
[18] Juang L-J, Gao X-Y, Mai S-T, Lee C-H, Lee M-C, Yao C-L. Safety assessment, biological effects, and mechanisms of Myrica rubra fruit extract for anti-melanogenesis, anti-oxidation, and free radical scavenging abilities on melanoma cells. J Cosmet Dermatol 2019;18(1):322–32. https://doi.org/10.1111/jocd.12505.
[19] Kim S, et al. Optimization of extraction condition of bee pollen using response surface methodology: correlation between anti-melanogenesis, antioxidant activity, and phenolic content. Molecules, 2015;20(11):19764–74.
[20] Li H, et al. Identification of anti-melanogenesis constituents from Morus alba L. leaves. Molecules, 2018;23(10):2559.
[21] Alberti KGMM, Zimmet P, Shaw J. Metabolic syndrome-a new world-wide definition. A Consensus Statement from the International Diabetes Federation. Diabet Med 2006;23(5):469–80. https://doi.org/10.1111/j.1464-5491.2006.01858.x.
[22] Executive Summary of The Third Report of The National Cholesterol Education Program (NCEP) Expert Panel on Detection, Evaluation, And Treatment of High Blood Cholesterol In Adults (Adult Treatment Panel III). Jama, 2001;285(19):2486–97.
[23] Faccio G, Kruus K, Saloheimo M, Thöny-Meyer L. Bacterial tyrosinases and their applications. Process Biochem 2012;47(12):1749–60. https://doi.org/10.1016/j.procbio.2012.08.018.
[24] Bourquelot E, Bertrand G. Le bleuissement et le noircissement des champignons. CR Soc Biol 1895;47:582–4.
[25] Feng L, Shi N, Cai S, Qiao X, Chu P, Wang H, Long F, Yang H, Yang Y, Wang Y, Yu H. De Novo Molecular Design of a Novel Octapeptide That Inhibits In Vivo Melanogenesis and Has Great Transdermal Ability. J Med Chem 2018;61(15):6846–57. https://doi.org/10.1021/acs.jmedchem.8b00737.s002.
[26] <Urolithin patent.pdf>.
[27] Arndt KA, Fitzpatrick TB. Topical use of hydroquinone as a depigmenting agent. JAMA 1965;194(9):965–7.
[28] Chang TS. An updated review of tyrosinase inhibitors. Int J Molecular Sci, 2009;10(6):2440–75.
[29] Cabanes J, Chazarra S, Garcia-Carmona F. Kojic acid, a cosmetic skin whitening agent, is a slow-binding inhibitor of catecholase activity of tyrosinase. J Pharmacy Pharmacol, 1994;46(12):982–5.
[30] Khatib S, Nerya O, Musa R, Shmuel M, Tamir S, Vaya J. Chalcones as potent tyrosinase inhibitors: the importance of a 2,4-substituted resorcinol moiety. Bioorg Med Chem 2005;13(2):433–41. https://doi.org/10.1016/j.bmc.2004.10.010.
[31] Jung HJ, Lee MJ, Park YJ, Noh SG, Lee AK, Moon KM, Lee EK, Bang EJ, Park YJ, Kim SJ, Yang J, Ullah S, Chun P, Jung YS, Moon HR, Chung HY. A novel synthetic compound, (Z)-5-(3-hydroxy-4-methoxybenzylidene)-2-iminothiazolidin-4-one (MHY773) inhibits mushroom tyrosinase. Biosci Biotechnol Biochem 2018;82(5):759–67. https://doi.org/10.1080/09168451.2018.1445518.
[32] Kim SJ, Yang J, Lee S, Park C, Kang D, Akter J, Ullah S, Kim Y-J, Chun P, Moon HR. The tyrosinase inhibitory effects of isoxazolone derivatives with a (Z)-β-phenyl-α, β-unsaturated carbonyl scaffold. Bioorg Med Chem 2018;26(14):3882–9. https://doi.org/10.1016/j.bmc.2018.05.047.
[33] Do Hyun Kim SJK, et al. Design, synthesis, and antimelanogenic effects of (2-substituted phenyl-1, 3-dithiolan-4-yl) methanol derivatives. Drug design, development and therapy, 2017;11:827.
[34] Yun HY et al. Design, synthesis, and anti-melanogenic effects of (E)-2-benzoyl-3-(substituted phenyl) acrylonitriles. Drug design, development and therapy 2015;9:4259.
[35] Halaouli S, Asther M, Sigoillot J-C, Hamdi M, Lomascolo A. Fungal tyrosinases: new prospects in molecular characteristics, bioengineering and biotechnological applications. J Appl Microbiol 2006;100(2):219–32. https://doi.org/10.1111/j.1365-2672.2006.02866.x.
[36] Barneda-Zahonero B, Parra M. Histone deacetylases and cancer. Mol Oncol 2012;6(6):579–89.
[37] N.P. Seeram, D.H., Therapeutic uses of urolithins. 2007. p. WO 2007127263 A2.
[38] Choi J, Jee JG. Repositioning of Thiourea-Containing Drugs as Tyrosinase Inhibitors. Int J Molecular Sci, 2015;16(12):28534–48.
[39] Campos Júlia Furtado, Pereira Michelly Cristiny, de Sena Wanessa Layssa Batista, de Barros Martins Caio Gomes, de Oliveira Jamerson Ferreira, da Cruz Amorim Cezar Augusto, de Melo Rêgo Moacyr Jesus Barreto, da Rocha Pitta Marina Galdino, de Lima Maria do Carmo Alves, da Rocha Pitta Maira Galdino, da Rocha Pitta Ivan. Synthesis and in vitro anticancer activity of new 2-thioxo-oxazolidin-4-one derivatives. Pharmacol Rep 2017;69(4):633–41. https://doi.org/10.1016/j.pharep.2017.03.005.
[40] Jiang Shibo, Tala Srinivasa R, Lu Hong, Zou Peng, Avan Ilker, Ibrahim Tarek S, Abo-Dya Nader E, Abdelmajeid Abdelmotaal, Debnath Asim K, Katritzky Alan R. Design, synthesis, and biological activity of a novel series of 2,5-disubstituted furans/pyrroles as HIV-1 fusion inhibitors targeting gp41. Bioorg Med Chem Lett 2011;21(22):6895–8. https://doi.org/10.1016/j.bmcl.2011.08.081.
[41] Harada Koichiro, Kubo Hideki, Tanaka Akio, Nishioka Kazuhiko. Identification of oxazolidinediones and thiazolidinediones as potent 17β-hydroxysteroid dehydrogenase type 3 inhibitors. Bioorg Med Chem Lett 2012;22(1):504–7. https://doi.org/10.1016/j.bmcl.2011.10.095.
[42] Mourão RH, Silva TG, Soares ALM, Vieira ES, Santos JN, Lima MCA, Lima VLM, Galdino SL, Barbe J, Pitta IR. Synthesis and Biological Activity of Novel Acridinylidene and Benzylidene thiazolidinediones. Eur J Med Chem 2005;40(11):1129–33. https://doi.org/10.1016/j.ejmech.2005.06.002.
[43] Chung Ki Wung, Jeong Hyoung Oh, Jang Eun Ji, Choi Yeon Ja, Kim Dae Hyun, Kim So Ra, Lee Kyung Jin, Lee Hye Jin, Chun Pusoon, Byun Youngjoo, Moon

Hyung Ryong, Chung Hae Young. Characterization of a small molecule inhibitor of melanogenesis that inhibits tyrosinase activity and scavenges nitric oxide (NO). Biochimica et Biophysica Acta (BBA) - General Subjects 2013;1830(10):4752–61. https://doi.org/10.1016/j.bbagen.2013.06.002.

[44] Choi Yeon Ja, Uehara Yohei, Park Ji Young, Kim Seong Jin, Kim So Ra, Lee Hee Won, Moon Hyung Ryong, Chung Hae Young. MHY884, a newly synthesized tyrosinase inhibitor, suppresses UVB-induced activation of NF-κB signaling pathway through the downregulation of oxidative stress. Bioorg Med Chem Lett 2014;24(5):1344–8. https://doi.org/10.1016/j.bmcl.2014.01.040.

[45] Kim Hye Rim, Lee Hye Jin, Choi Yeon Ja, Park Yun Jung, Woo Youngwoo, Kim Seong Jin, Park Min Hi, Lee Hee Won, Chun Pusoon, Chung Hae Young, Moon Hyung Ryong. Benzylidene-linked thiohydantoin derivatives as inhibitors of tyrosinase and melanogenesis: importance of the β-phenyl-α,β-unsaturated carbonyl functionality. Med Chem Commun 2014;5(9):1410–7. https://doi.org/10.1039/C4MD00171K.

[46] Kim So Hee, Ha Young Mi, Moon Kyoung Mi, Choi Yeon Ja, Park Yun Jung, Jeong Hyoung Oh, Chung Ki Wung, Lee Hye Jin, Chun Pusoon, Moon Hyung Ryong, Chung Hae Young. Anti-melanogenic effect of (Z)-5-(2,4-dihydroxybenzylidene) thiazolidine-2,4-dione, a novel tyrosinase inhibitor. Arch Pharm Res 2013;36(10):1189–97. https://doi.org/10.1007/s12272-013-0184-5.

[47] Son Sujin, Kim Haewon, Yun Hwi Young, Kim Do Hyun, Ullah Sultan, Kim Seong Jin, Kim Yeon-Jeong, Kim Min-Soo, Yoo Jin-Wook, Chun Pusoon, Moon Hyung Ryong. (E)-2-Cyano-3-(substituted phenyl)acrylamide analogs as potent inhibitors of tyrosinase: A linear β-phenyl-α,β-unsaturated carbonyl scaffold. Bioorg Med Chem 2015;23(24):7728–34. https://doi.org/10.1016/j.bmc.2015.11.015.

[48] Kang KH et al. (Z)-2-(Benzo [d] thiazol-2-ylamino)-5-(substituted benzylidene) thiazol-4 (5H)-one Derivatives as Novel Tyrosinase Inhibitors. Biol Pharm Bull 2015;38(8):1227–33.

[49] Chung Ki Wung, Park Yun Jung, Choi Yeon Ja, Park Min Hi, Ha Young Mi, Uehara Yohei, Yoon Jung Hyun, Chun Pusoon, Moon Hyung Ryong, Chung Hae Young. Evaluation of in vitro and in vivo anti-melanogenic activity of a newly synthesized strong tyrosinase inhibitor (E)-3-(2,4 dihydroxybenzylidene) pyrrolidine-2,5-dione (3-DBP). Biochimica et Biophysica Acta (BBA) - General Subjects 2012;1820(7):962–9. https://doi.org/10.1016/j.bbagen.2012.03.018.

[50] Han Yu Kyeong, Park Yun Jung, Ha Young Mi, Park Daeui, Lee Ji Yeon, Lee Naree, Yoon Jeong Hyun, Moon Hyung Ryong, Chung Hae Young. Characterization of a novel tyrosinase inhibitor, (2RS,4R)-2-(2,4-dihydroxyphenyl)thiazolidine-4-carboxylic acid (MHY384). Biochimica et Biophysica Acta (BBA) - General Subjects 2012;1820(4):542–9. https://doi.org/10.1016/j.bbagen.2012.01.001.

[51] Ullah Sultan, Park Yujin, Park Chaeun, Lee Sanggwon, Kang Dongwan, Yang Jungho, Akter Jinia, Chun Pusoon, Moon Hyung Ryong. Antioxidant, anti-tyrosinase and anti-melanogenic effects of (E)-2,3-diphenylacrylic acid derivatives. Bioorg Med Chem 2019;27(11):2192–200. https://doi.org/10.1016/j.bmc.2019.04.020.

[52] Ullah Sultan, Akter Jinia, Kim Su J, Yang Jungho, Park Yujin, Chun Pusoon, Moon Hyung R. The tyrosinase-inhibitory effects of 2-phenyl-1,4-naphthoquinone analogs: importance of the (E)-β-phenyl-α,β-unsaturated carbonyl scaffold of an endomethylene type. Med Chem Res 2019;28(1):95–103. https://doi.org/10.1007/s00044-018-2267-9.

[53] Ullah Sultan, Kang Dongwan, Lee Sanggwon, Ikram Muhammad, Park Chaeun, Park Yujin, Yoon Sik, Chun Pusoon, Moon Hyung Ryong. Synthesis of cinnamic amide derivatives and their anti-melanogenic effect in α-MSH-stimulated B16F10 melanoma cells. Eur J Med Chem 2019;161:78–92. https://doi.org/10.1016/j.ejmech.2018.10.025.

[54] Ullah Sultan, Park Yujin, Ikram Muhammad, Lee Sanggwon, Park Chaeun, Kang Dongwan, Yang Jungho, Akter Jinia, Yoon Sik, Chun Pusoon, Moon Hyung Ryong. Design, synthesis and anti-melanogenic effect of cinnamamide derivatives. Bioorg Med Chem 2018;26(21):5672–81. https://doi.org/10.1016/j.bmc.2018.10.014.

[55] Vogeli U et al. C-13-Nmr Spectroscopy. 19. Structures of Addition-Products of Acetylene-Dicarboxylic Acid-Esters with Various Dinucleophiles - Application of C, H-Spin-Coupling Constants. Helv Chim Acta 1978;61(2):607–17.

[56] The UniProt Consortium. UniProt: the universal protein knowledgebase. Nucleic Acids Res 2016;45(D1):D158–69.

[57] Lai Xuelei, Wichers Harry J, Soler-Lopez Montserrat, Dijkstra Bauke W. Structure of Human Tyrosinase Related Protein 1 Reveals a Binuclear Zinc Active Site Important for Melanogenesis. Angew Chem Int Ed 2017;56(33):9812–5. https://doi.org/10.1002/anie.201704616.

[58] Hyun Sook Kyung, Lee Won-Hee, Jeong Da Mi, Kim Youngsoo, Choi Jae Sue. Inhibitory Effects of Kurarinol, Kuraridinol, and Trifolirhizin from Sophora flavescens on Tyrosinase and Melanin Synthesis. Biol Pharm Bull 2008;31(1):154–8. https://doi.org/10.1248/bpb.31.154.

[59] Morris Garrett M, Goodsell David S, Halliday Robert S, Huey Ruth, Hart William E, Belew Richard K, Olson Arthur J. Automated docking using a Lamarckian genetic algorithm and an empirical binding free energy function. J Comput Chem 1998;19(14):1639–62. https://doi.org/10.1002/(SICI)1096-987X(19981115)19:14<1639::AID-JCC10>3.0.CO;2-B.

[60] Friesner RA et al. Extra precision glide: Docking and scoring incorporating a model of hydrophobic enclosure for protein− ligand complexes. J Med Chem 2006;49(21):6177–96.

[61] Farid Ramy, Day Tyler, Friesner Richard A, Pearlstein Robert A. New insights about HERG blockade obtained from protein modeling, potential energy mapping, and docking studies. Bioorg Med Chem 2006;14(9):3160–73. https://doi.org/10.1016/j.bmc.2005.12.032.

[62] Bae Sung Jin, Ha Young Mi, Kim Jin-Ah, Park Ji Young, Ha Tae Kwun, Park Daeui, Chun Pusoon, Park Nam Hee, Moon Hyung Ryong, Chung Hae Young. A Novel Synthesized Tyrosinase Inhibitor: (E)-2-((2,4-Dihydroxyphenyl)diazenyl)phenyl 4-Methylbenzenesulfonate as an Azo-Resveratrol Analog. Biosci Biotechnol Biochem 2013;77(1):65–72. https://doi.org/10.1271/bbb.120547.

[63] Chen Lih-Geeng, Chang Wei-Ling, Lee Chia-Jung, Lee Lain-Tze, Shih Chwen-Ming, Wang Ching-Chiung. Melanogenesis Inhibition by Gallotannins from Chinese Galls in B16 Mouse Melanoma Cells. Biol Pharm Bull 2009;32(8):1447–52. https://doi.org/10.1248/bpb.32.1447.